Journal of Medicinal Chemistry

pubs.acs.org/jmc Article

The Development of Hsp90β-Selective Inhibitors to Overcome Detriments Associated with *pan*-Hsp90 Inhibition

Sanket J. Mishra, Weiya Liu, Kristin Beebe, Monimoy Banerjee, Caitlin N. Kent, Vitumbiko Munthali, John Koren, III, John A Taylor, III, Leonard M. Neckers, Jeffrey Holzbeierlein, and Brian S. J. Blagg*

Cite This: *J. Med. Chem.* 2021, 64, 1545−1557 Read Online

ACCESS | Metrics & More | Article Recommendations | Supporting Information

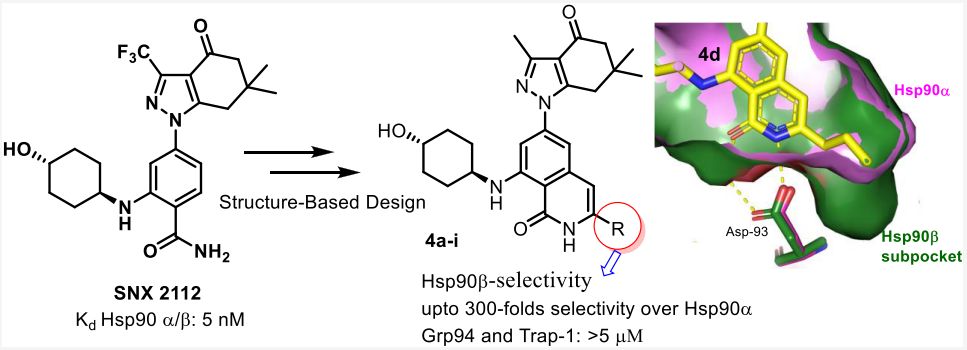

ABSTRACT: The 90 kD heat shock proteins (Hsp90) are molecular chaperones that are responsible for the folding of select proteins, many of which are directly associated with cancer progression. Consequently, inhibition of the Hsp90 protein folding machinery results in a combinatorial attack on numerous oncogenic pathways. Seventeen small-molecule inhibitors of Hsp90 have entered clinical trials for the treatment of cancer, all of which bind the Hsp90 N-terminus and exhibit *pan*-inhibitory activity against all four Hsp90 isoforms, which may lead to adverse effects. The development of Hsp90 isoform-selective inhibitors represents an alternative approach toward the treatment of cancer and may limit some of these detriments. Described herein, is a structure-based approach to develop isoform-selective inhibitors of Hsp90*β*, which induces the degradation of select Hsp90 clients without concomitant induction of Hsp90 levels. Together, these initial studies support the development of Hsp90*β*-selective inhibitors as a method for overcoming the detriments associated with *pan*-inhibition.

INTRODUCTION

The molecular chaperone, heat shock protein 90 kDa (Hsp90), regulates cellular homeostasis by assisting in the maturation of nascent polypeptides, the refolding of denatured proteins, and the disaggregation of protein aggregates.[1−3] Hsp90 modulates the conformation of more than 300 client protein substrates into their biologically active conformation. Many of these client proteins, such as signaling proteins, are drivers of cancer progression, initiation, and/or metastasis.[2] In fact, Hsp90's clients are associated with all 10 hallmarks of cancer, and in principle, Hsp90 inhibition should mimic the effects of combination therapy.[3,4] As a result, Hsp90 has emerged as a promising target for the development of anti-cancer agents.[3−10]

Hsp90 as a chemotherapeutic target is further supported by its upregulation during malignant transformation, maintenance, and progression.[11−13] Despite its abundance in normal tissues, Hsp90 can be targeted selectively in tumor cells due to increased levels of the Hsp90 heteroprotein complex that resides within cancer cells and possesses >200-fold higher affinity for ATP/inhibitors than the Hsp90 homodimer found in normal cells.[9] Consequently, Hsp90 inhibitors accumulate in tumor cells at significantly higher concentrations than normal tissues and exhibit a large therapeutic window. As a result, Hsp90 has been extensively sought after as a therapeutic target for the treatment of cancer and, ultimately, led to the investigation of 17 clinical candidates.[14−17] Unfortunately, the clinical evaluation of these inhibitors has produced a number of complications.[18−23] Detriments observed with current Hsp90 inhibitors include the lack of translational efficacy, induction of the heat shock response (HSR) that produces increased levels of Hsp90, and on-target toxicities amongst others. Hsp90 inhibitors that have undergone clinical investigation for the treatment of cancer bind the N-terminal nucleotide-binding site and inhibit all four Hsp90 isoforms (*pan*-inhibition) with similar affinity.[24−26] The Hsp90ß

Received: September 28, 2020
Published: January 11, 2021

https://dx.doi.org/10.1021/acs.jmedchem.0c01700
J. Med. Chem. 2021, 64, 1545−1557

isoform is constitutively expressed in the cytoplasm, whereas Hsp90α is inducible and expressed in the cytosol upon exposure to cellular stress. The organelle-specific isoforms glucose-regulated protein 94 (Grp94) reside in the endoplasmic reticulum, and tumor necrosis factor receptor-associated protein 1 (Trap-1) is localized to the mitochondria.[1−3] Recent studies have shown that maturation and trafficking of the hERG channel is solely dependent upon the Hsp90α isoform, suggesting that inhibition of Hsp90α is likely to contribute toward the cardio and ocular toxicities observed in clinical trials.[23] Consequently, isoform-selective inhibitors may prove useful to identify isoform-dependent substrates and overcome the liabilities associated with *pan*-inhibition.

Hydrolysis of ATP by the N-terminal nucleoside-binding pocket provides the requisite energy needed for the maturation of client protein substrates, and all four Hsp90 isoforms share >85% identity within this region.[27−31] In fact, 21 of the 29 residues within this pocket are totally conserved, and the remaining 8 share a high degree of similarity. Grp94 manifests the lowest identity within the N-terminal-binding site, as Grp94 exhibits a unique structural feature that results from a five-amino acid insertion into the primary sequence, which translates into a Grp94-exclusive binding pocket. Prior studies exploited the Grp94-exclusive binding pocket and led to isoform-selective inhibitors, which have revealed unexpected therapeutic opportunities for Grp94-selective inhibition.[32−34] As a result, multiple scaffolds that manifest selective Grp94 inhibition have now been disclosed. In contrast, Hsp90α and Hsp90ß share ∼95% identity within this region and only two amino acids differ between these isoforms, making the development of Hsp90α- or Hsp90ß-selective inhibitors very challenging.[30,31] **KUNB31** (Figure 1) represents the first Hsp90ß isoform-selective inhibitor discovered, which was achieved by taking advantage of subtle differences between the Hsp90α and Hsp90β co-crystal structures and analysis of the conserved water molecules that reside within these regions.[35] Remarkably, **KUNB31** was shown to induce the degradation of Hsp90β-dependent clients without concomitant induction of Hsp90 levels, providing an alternate approach for the treatment of cancer that addresses two of the major detriments associated with *pan*-Hsp90 inhibitors (Hsp90 induction and hERG maturation).[35]

Sequence alignment of the residues that form the Hsp90α and Hsp90β N-terminal ATP-binding pockets revealed Hsp90β to contain Ala52 and Leu91 in lieu of Ser52 and Ile91, which are present in Hsp90α (Figure 1A,B). Substitution of these two amino acids results in a small and extended binding pocket in Hsp90β (Figure 1A,B) due to the increased flexibility of Leu91, unlike Ile91 in Hsp90α (Figure 1A).[31,35] In addition, all four Hsp90 isoforms contain a water-mediated hydrogen bond network in close proximity to Asp93 that facilitates Hsp90's interactions with ligands, as shown in Figure 1A,B. In silico overlay of the Hsp90α and Hsp90β co-crystal structures indicate, these water molecules play a different role in each isoform. Ser52 is replaced with Ala52 in Hsp90β and forms a hydrogen bond with bound water molecule **A**, whereas Ala52 does not participate in the hydrogen-bonding network. Therefore, it was hypothesized that Hsp90β-selective inhibitors could be developed via the introduction of substituents that sterically clash with Ile91 in Hsp90α and, consequently, disrupt the water-mediated hydrogen-bonding network.

KUNB31 is a ring-constrained variant of substitutions at the 3- and 4-positions, which were designed to minimize the

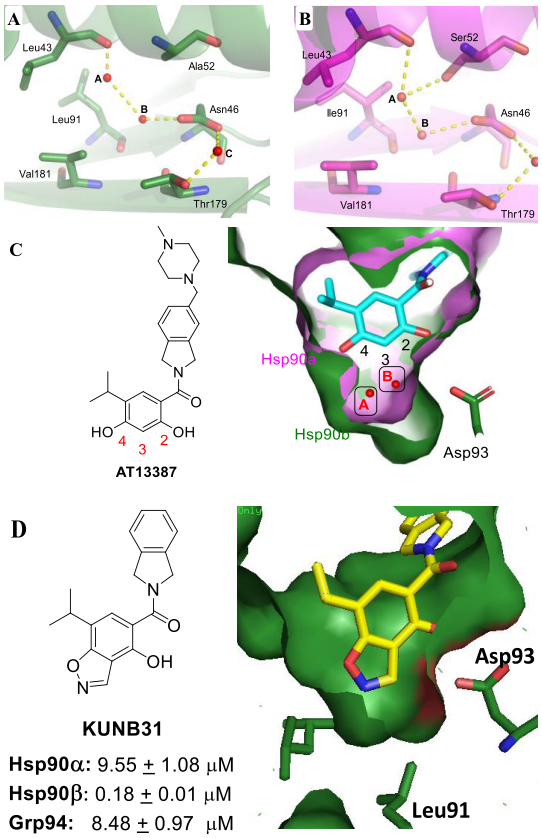

Figure 1. Water-mediated network of hydrogen bonds. (A) Hydrogen-bonding network at the bottom of the Hsp90β pocket (PDB code: 1UYM). (B) Hydrogen-bonding network in the bottom of the Hsp90α-binding pocket (PDB code: 2XAB). (C) Two-dimensional representation of the Hsp90β-binding pocket with the known *pan*-inhibitor AT11387. (D) **KUNB31** bound to Hsp90β with apparent Kd values observed in fluorescence polarization assay (PDB code: 5UCJ).

entropic penalty upon binding Hsp90β, while simultaneously displacing water molecules **A** and **B** (visible in Figure 1). **KUNB31** was found to manifest an apparent Kd of 180 nM against Hsp90β and ∼50-fold selectivity versus other Hsp90 isoforms. Through solution of the co-crystal structure, it was confirmed that **KUNB31** displaced both water molecules and validated this approach toward the development of Hsp90β-selective inhibitors. Based on these observations, a new scaffold was pursued in an effort to improve both affinity and selectivity for Hsp90ß. Reported herein, is the rational development of an isoquinolin-1(2*H*)-one-containing inhibitor that selectively binds the Hsp90β isoform with nanomolar affinity and exhibits greater than 200-fold selectivity versus other Hsp90 isoforms.

RESULTS AND DISCUSSION

SNX 2112 is a benzamide-containing Hsp90 inhibitor that was previously reported (Figure 2A) and shown to exhibit equipotent affinity for both Hsp90α and Hsp90β (Figure 2A).[36] Subsequent optimization by Vertex Pharmaceuticals led to **31**, which manifests selective inhibition of both Hsp90α and Hsp90β without affinity for Grp94 and Trap1. The co-crystal structure of **31** (PDB code: 4O0B) bound to Hsp90α was overlaid with the Hsp90β co-crystal structure (PDB code: 1UYM), which revealed **31** does not interfere with the conserved water molecules found in the Hsp90α/β pockets

https://dx.doi.org/10.1021/acs.jmedchem.0c01700
J. Med. Chem. 2021, 64, 1545−1557

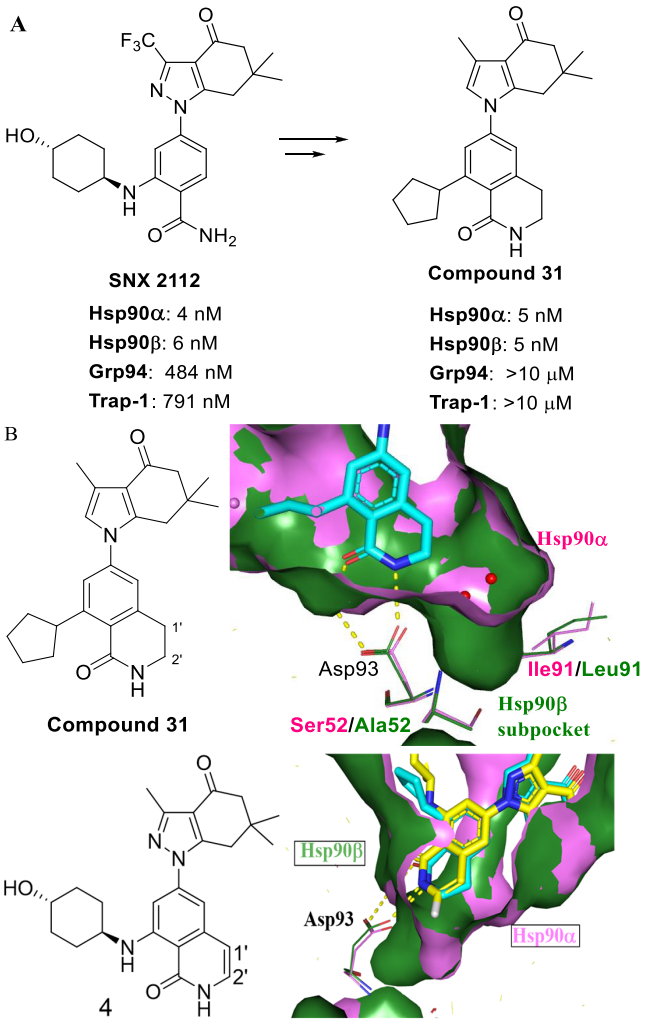

Figure 2. (A) Structures and IC50's of the benzamide-based Hsp90 inhibitors SNX 2112 and compound **31** in the FP assay. (B) Alignment of compound **4** (yellow) and compound **31** modeled into the Hsp90*α* (PDB code: 4O0B) and Hsp90ß (PDB code: 1UYM) ATP-binding pockets.

(depicted as red spheres in Figure 1, labeled as **A** and **B** in Figure 1C). Compound **31** also contains a ring-constrained benzamide group, which appears to lock the amide into a rigid conformation to facilitate interactions with Asp93.[38] Molecular modelling studies with **31** suggested that modifications to the 2′-position (Figure 2A,B) could displace the conserved water molecules and extend into the Hsp90*β* subpocket and produce Hsp90ß-selective inhibition.

In addition to modifications at the 2-position, the cyclopentyl group was replaced with a *trans*-4-cylcohexanolamine to enhance occupation and increase solubility. The tetrahydroindazolone fragment was also incorporated in lieu of the pyrazolone present in compound **31**, as it does not change affinity significantly. The unsaturated alkene was used to explore the spatial constraints of the Hsp90*β*-subpocket, as computational studies supported that its introduction would allow the benzamide to maintain key interactions with Asp93 (Figure 2A). The 2′-position substitutions in the proposed compound series represented by **4** (Figure 2B) appeared to project toward the Hsp90*β*-specific subpocket, allowing investigation of this subpocket as depicted in Figure 2B. Given the hydrophobic nature of the Hsp90*β* subpocket, linear aliphatic chains were attached to the 2′-position for investigation of the initial analogues. In addition, methyl ethers and alcohols were attached to the 2′-position to probe for beneficial interactions with Leu-48 (in both *α* and *β*) and/or Ser-52 in Hsp90*α*.

Synthesis of these analogues commenced via installation of the saturated indazolone (Scheme 1).

2,4,6-Trifluorobenzonitrile (**1**) was treated with hydrazine hydrate and 2-acetyl dimedone to produce **2**, which was subsequently exposed to a variety of *β*-ketoesters that contained the desired R-groups in the presence of potassium carbonate to ultimately give the *β*-ketoester-substituted benzonitriles. The resulting benzonitriles underwent condensation and cyclization reactions upon treatment with acetic acid and sulfuric acid to yield intermediates **3a**−**3i**. The *trans*-4-aminocyclohexanol moiety was installed via an SNAr reaction in the presence of diisopropylethylamine to furnish the final products, **4a**−**i**. Compound **3j** was prepared upon the exposure of **3i** with boron tribromide, and installation of the amine on **3j** yielded **4j** (Scheme 2).

Compounds **5a**−**5g** were prepared from **3d** via the reaction conditions described in Scheme 3.

Once prepared, the compounds were evaluated for their binding affinities against the cytosolic isoforms, Hsp90*α* and Hsp90*β*, by measuring their ability to competitively displace FITC-labeled geldanamycin (GDA) in a fluorescence polarization assay (IC_{50}'s listed in Table 1).[37]

The first compound in the series, **4a**, contained a methyl at the 2′-position and exhibited 3-fold selectivity for Hsp90ß, suggesting that further modification could enhance selectivity. Elongation of the chain to include an ethyl appendage (**4b**) enhanced affinity for both Hsp90*α* and Hsp90ß, which occurs by occupation of the subpocket in both isoforms. An isopropyl group was installed to generate **4c**, which maintained a similar affinity and selectivity as **4b** and established that a branched aliphatic chain could be accommodated within the subpocket. Increasing the chain length to the propyl derivative (**4d**) led to an improvement in both affinity and selectivity, as **4d** manifested ∼40 nM IC_{50} for Hsp90*β* and ∼21-fold selectivity over Hsp90*α*. In addition, **4d** exhibited a decreased binding affinity toward Trap-1 and Grp94 (>50 *μ*M for both isoforms, SI). Encouraged by these results, a butyl chain was incorporated to probe the depth of the Hsp90*β* subpocket. Expectedly, the *n*-butyl group (**4e**) was found to exhibit excellent selectivity for Hsp90*β* (>300-fold vs Hsp90*α*) but a reduced affinity (IC_{50} = 186 nM). Since the isopropyl group was accommodated in both Hsp90*α* and Hsp90*β*, a *t*-butyl appendage was attached (**4f**) to determine whether the pocket could accommodate spherical bulk. Compound **4e** did not bind either isoform. Compound **4g** was synthesized to contain an isobutyl group, which maintained selectivity, but also led to a decrease in affinity. A cyclopropyl group was also evaluated (**4h**), and a loss of potency was observed as compared to **4c**. Surprisingly, compounds **4i** and **4j** displayed a loss of selectivity for Hsp90*β* over Hsp90*α* but also contained polar appendages.

Computational studies suggested that replacement of the *trans*-4-aminocyclohexanolamine with other surrogates may alter the binding conformation and, thus, affinity and selectivity. Therefore, multiple amines were investigated that incorporated various functional groups, including ionizable tertiary amines to improve solubility. The computationally derived binding mode for **5a**, a morpholine-containing

https://dx.doi.org/10.1021/acs.jmedchem.0c01700
J. Med. Chem. 2021, 64, 1545−1557

Scheme 1. (a) $NH_2NH_2 \cdot H_2O$, Ethanol, 60° C. (b) 2-Acetyldimedone, Ethanol, Reflux. (c) β-ketoester, K_2CO_3, DMF, 70° C. (d) H_2SO_4/Water/Acetic Acid (2:1:7), 130 °C, 6 h. (e) *trans*-Cyclohexanolamine, DIPEA, DMSO, 140° C, 12 h

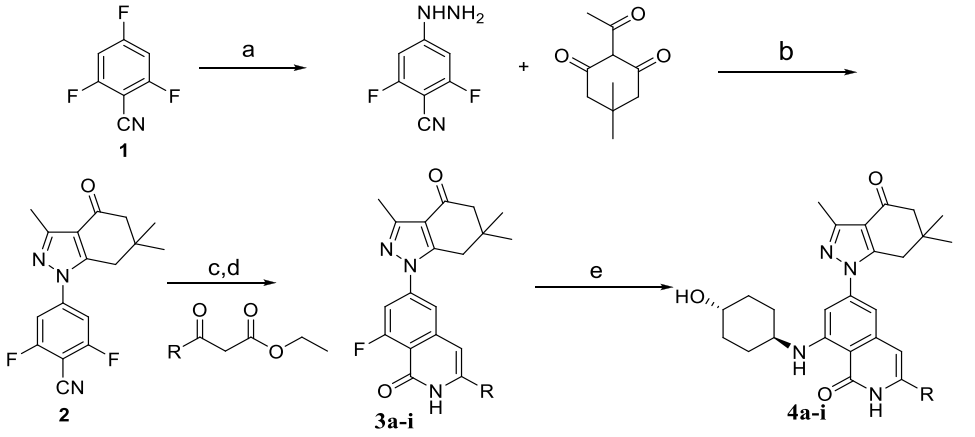

3a ,4a: R=Methyl
3b, 4b: R=Ethyl
3c, 4c: R=Isopropyl
3d, 4d: R=Propyl
3e, 4e: R=Butyl
3f, 4f: R= *t*-butyl
3g, 4g: R= Isobutyl
3h, 4h: R= Cyclopropyl
3i, 4i: R= CH_2OCH_3

Scheme 2. Syntheses of 3j and 4j; (a) BBr_3, DCM, 0 °C. (b) *trans*-4-aminocyclohexanol, DIPEA, DMSO, 140 °C

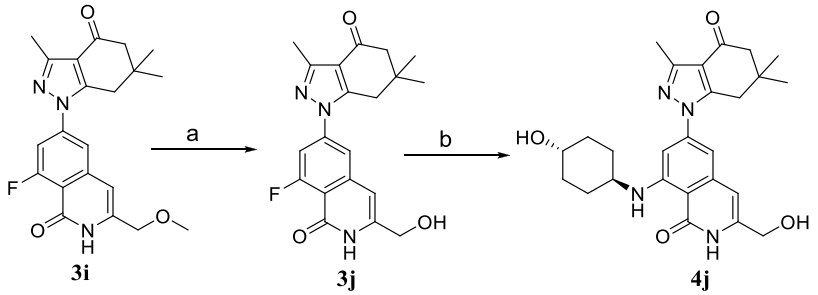

Scheme 3. Syntheses of 5a−5g (a) Amine, DIPEA, DMSO, 140 °C

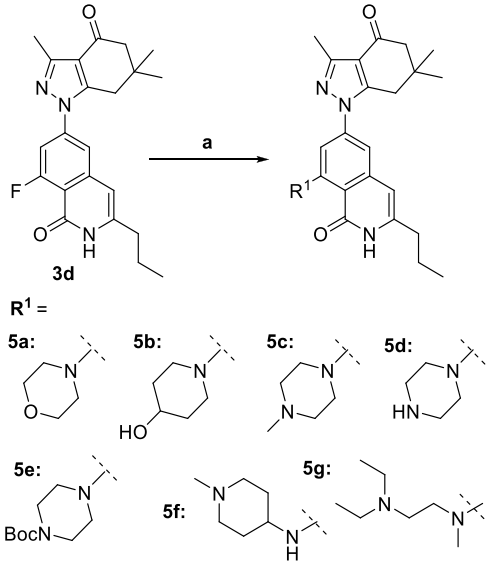

Table 1. IC50 Values of Compounds 4a−4j against Hsp90α and Hsp90β Determined Using Fluorescence Polarization (FP) Assay

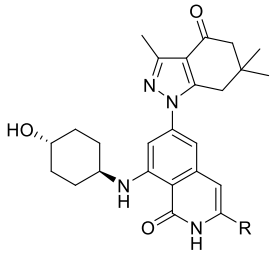

entry	R	Hsp90α IC_{50} (μM)	Hsp90β IC_{50} (μM)
4a	methyl	0.294 ± 0.023	0.101 ± 0.003
4b	ethyl	0.180 ± 0.036	0.068 ± 0.008
4c	isopropyl	0.173 ± 0.036	0.051 ± 0.008
4d	propyl	0.886 ± 0.040	0.040 ± 0.003
4e	*n*-butyl	>50	0.156 ± 0.018
4f	*t*-butyl	>50	>50
4g	isobutyl	>50	0.264 ± 0.030
4h	cyclopropyl	1.88 ± 0.28	0.946 ± 0.038
4i	$-CH_2OCH_3$	0.306 ± 0.023	0.159 ± 0.003
4j	$-CH_2OH$	0.824 ± 0.104	0.233 ± 0.018

compound, is presented in Figure 3 and suggests a slight rotation of the isoquino-lin-1(2*H*)-one ring, which appears to result from disfavored interactions between the morpholine ring and protein surface. This conformational change appears to align the 2′-appendage at an angle that is neither optimized for selectivity nor affinity. An additional reason to replace the *trans*-4-aminocyclohexanol is to disrupt the planarity that is

https://dx.doi.org/10.1021/acs.jmedchem.0c01700
J. Med. Chem. 2021, 64, 1545−1557

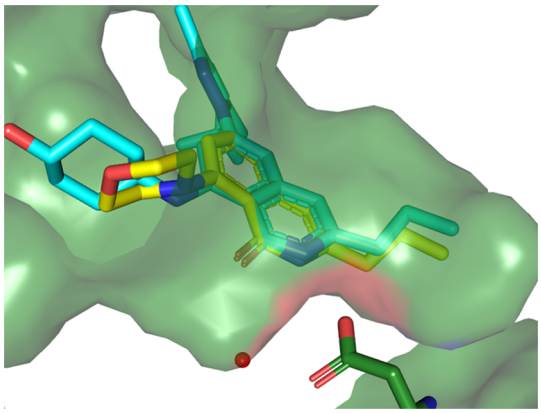

Figure 3. Overlay of proposed binding modes of **4d** (cyan) and **5a** (yellow) in Hsp90β (PDB code: 1UYM).

caused by the intramolecular hydrogen bond between the aniline and carbonyl moieties, which is likely to affect solubility.

Upon their preparation, compounds **5a**−**5g** were evaluated for their binding affinities against the cytosolic Hsp90 isoforms (Table 2). The binding profile of the morpholine-containing compound, **5a**, was consistent with the proposed hypothesis and exhibited excellent selectivity for Hsp90β with a IC50 of ∼121 nM. The binding profile for **5a** mirrored **4e**, which contains an *n*-butyl group at the 2′-position.

This data suggests that, with **5a**, the propyl chain aligns in Hsp90β in a manner similar to the butyl chain of **4e** and, thus, increases selectivity. Compound **5b**, which contains an alcohol, was proposed to interact with the amino acids at the gate of the binding pocket, such as Gly-97 and Lys-58. Alcohol **5b** was found to exhibit ∼91 nM IC_{50} for Hsp90β with >400-fold selectivity over Hsp90α, which supports the proposed binding model. Incorporation of *N*-methyl piperazine (**5c**) led to a decrease in affinity and selectivity as compared to **5a** and **5b**, which is likely to result from unfavorable interactions with Lys-58, which is present in both isoforms. Similarly, compounds **5d**−**5g** manifested reduced affinity for Hsp90β. Based on the proposed binding model, it appears that the carbonyl electrons could participate in stronger hydrogen-bonding interactions if the lactam was more flexible. In addition, this flexibility would allow appendages at the 2-position to project more efficiently into the Hsp90β-specific subpocket. Therefore, the saturated lactams **6a** and **6b** were pursued and are shown in Figure 4.

Table 2. IC_{50} Values for Compounds 5a−5g against Hsp90α and Hsp90β Determined via Fluorescence Polarization (FP) Assay

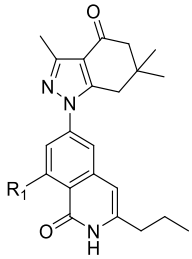

5a-g

entry	Hsp90α IC_{50} (μM)	Hsp90β IC_{50} (μM)
5a	>50	0.121 ± 0.017
5b	38.00 ± 1.10	0.091 ± 0.010
5c	8.52 ± 0.24	0.426 ± 0.053
5d	>50	4.47 ± 0.278
5e	>50	0.463 ± 0.031
5f	17.083 ± 0.66	0.513 ± 0.067
5g	>50	4.46 ± 0.188

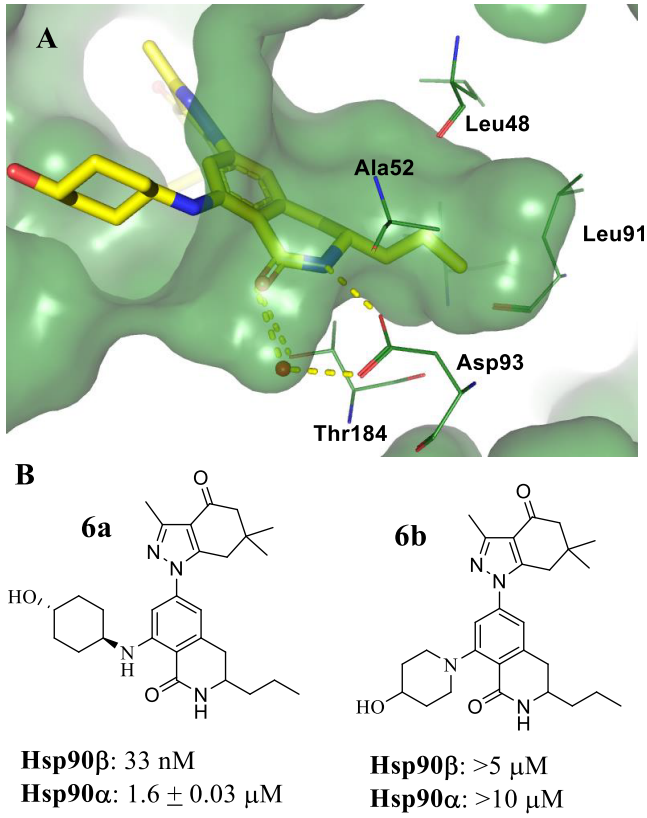

Figure 4. Proposed binding mode of **6a** in the Hsp90β-binding site (PDB code: 1UYM). (B) Structures and IC50 values of **6a** and **6b** determined using the FP assay.

Upon preparation as racemic mixtures (Scheme 4), **6a** and **6b** were evaluated; **6a** was shown to exhibit increased binding affinity as well as enhanced selectivity in comparison with **4d**, while **6b** lost both selectivity and affinity.

Compounds **4d** and **6a** were evaluated for their inhibitory activity against the NCI-60 cancer cell line panel and shown to manifest potent inhibition of select cancers. Interestingly, **4d** exhibited GI50's below 100 nM against several cancers, including, leukemia, colon, breast, and renal carcinoma. In

Scheme 4. (a) Pd/C, H_2 200 psi, Ethanol

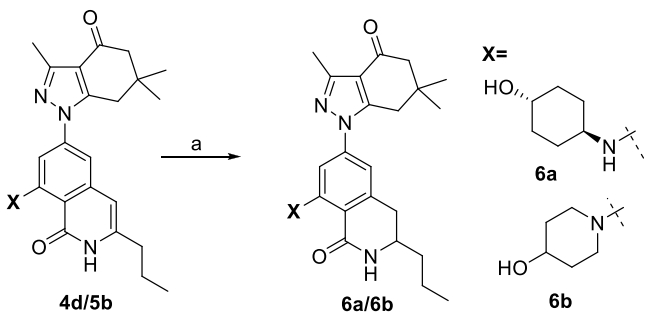

https://dx.doi.org/10.1021/acs.jmedchem.0c01700
J. Med. Chem. 2021, 64, 1545−1557

parallel, **4d** and **6a** were also evaluated for inhibitory activity against urological cancers, such as bladder and prostate cancers. As noted in Table 3, **4d** was found to manifest

Table 3. GI_{50} Values of 4d against Urological Cancer Cells

cancer type	cell line	GI_{50} (μM)
bladder cancer	UM-UC3	0.45 ± 0.08
	T24	0.196
prostate cancer	PC3-MM2	1.56 ± 0.24
	LNCap-LN3	1.07 ± 0.83
	C4-2B	1.42 ± 0.66
	LAPC-4	2.85 ± 0.41

GI50 values of ∼508 and ∼196 nM against UM-UC-3 and T24 bladder cancer cells, respectively, whereas the efficacy of **4d** against prostate cancer cells ranged between 1−2.5 μM.

Since Hsp90 inhibition induces the degradation of Hsp90-dependent substrates via the ubiquitin-proteosome pathway, the levels of both kinase and nonkinase Hsp90 clients were assessed via Western blot analysis (Figure 5). Known Hsp90

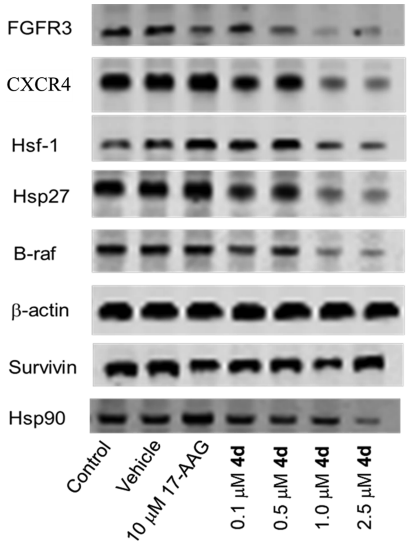

Figure 5. Western blot analysis of client proteins with **4d** in UM-UC-3 cells. 17-AAG (10 μM) was included as the positive control and the vehicle (DMSO) as the negative control.

clients, fibroblast growth factor receptor 3 (FGFR3) (highly mutated and/or overexpressed in nonmuscle-invasive urothelial carcinomas), CXCR4, and B-Raf, along with HSR elements Hsf-1 and Hsp27, were analyzed following the administration of **4d** to UM-UC-3 cells. After a 24 hour incubation with **4d**, Hsp90-dependent client proteins were reduced at concentrations that mirrored the cellular IC50 value (0.5 μM), clearly linking cell viability to Hsp90β inhibition (Figure 5).

A marked dose-dependent reduction of FGFR3 levels was observed alongside Hsp90β-dependent clients, CXCR4, and B-raf. Heat-shock-related proteins Hsp27 and Hsf-1 also declined upon increasing doses of **4d**, which mirrored the trend previously observed with the Hsp90β-selective compound, **KUNB31**. Survivin, which is an Hsp90α-dependent substrate was not affected, and it provides direct evidence for isoform-selective inhibition in the cellular context. The saturated derivative, **6a**, exhibited similar effects after 24 h exposure to HCT-116 cells (Figure 6, GI50 0.427 ± 0.07 μM). In addition,

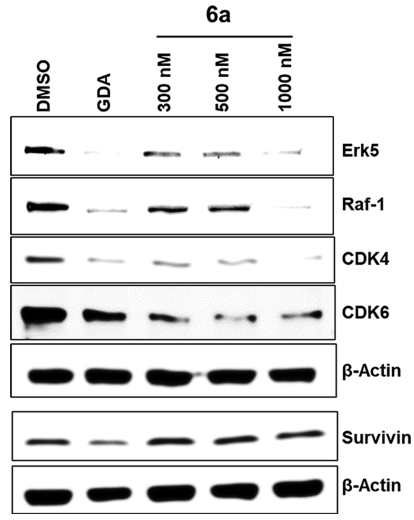

Figure 6. Western blot analysis of client proteins with **6a** in HCT-116 cells. Geldanamycin (GDA) (0.5 μM) was included as the positive control and the vehicle (DMSO) as the negative control.

6a induced the degradation of known Hsp90β-dependent clients such as CDK4 and CDK6. Total levels of Erk5 and Raf-1 also decreased at higher concentration of **6a**, while the Hsp90α-dependent substrate survivin was minimally affected, which provides further evidence for isoform-selective inhibition with the cellular environment.[39] The GI50 values obtained from in vitro evaluation against Hct116 and HEK293 cells suggest that an increase in hsp90β-selectivity results in a decrease in cytotoxicity (Table S2); however, the effect of physicochemical properties on cellular efficacy will require further investigation.

Since compound **5b** exhibited high selectivity for Hsp90β with IC50 ∼91 nM, it was evaluated in SkBr3 cells for its effectiveness on the maturation of proteins that drive oncogenesis (Figure 7). Hsp90α knockdown via Hsp90α siRNA was carried out to distinguish the roles of Hsp90α and Hsp90β on maturation of the known Hsp90 client, ErbB2 (HER2). HER2 belongs to the epidermal growth factor receptor family of proteins (EGFR) and exhibits intrinsic receptor tyrosine kinase activity that is overexpressed in ∼30% of the breast cancers and many other cancers. It is hypothesized in literature that plasma membrane-bound HER2 in SkBr3 cells is dependent upon Grp94; however, the cytosolic HER2 population is still maintained by Hsp90.[39−41] Compound **5b** was utilized as a chemical tool to inhibit Hsp90β, which revealed HER2 to be dependent upon both cytosolic isoforms, as the inhibition of Hsp90β with **5b** was not effective at reducing HER2 maturation (control siRNA, 18 h reading). However, upon knockdown of Hsp90α with siRNA in the presence of **5b**, the levels of HER2 were significantly reduced. Therefore, HER2 maturation exhibits redundant dependency upon both Hsp90 isoforms, and therefore, a functional loss of Hsp90β can be compensated for by Hsp90α for HER2. Unlike the *pan*-inhibitor, GDA, **5b** did not induce the heat-shock response even at 10 μM (control siRNA, 18 h), which is an attribute of Hsp90β-selective inhibitors. In addition, known Hsp90β-dependent clients such as CDK4 and c-IAP1 were degraded in a dose-dependent manner upon increasing concentrations of **5b**, but they were unaffected by Hsp90α knockdown.

https://dx.doi.org/10.1021/acs.jmedchem.0c01700
J. Med. Chem. 2021, 64, 1545−1557

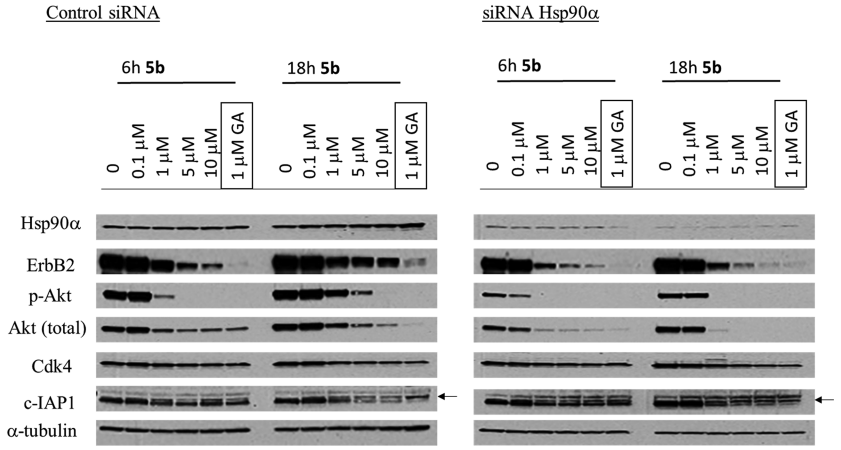

Figure 7. Western blot analysis of **5b** to study client protein degradation in SkBr3 cells, GA: gambogic acid.

CONCLUSIONS

Hsp90 inhibitors that have undergone clinical evaluation bind the Hsp90 N-terminal ATP-binding site and manifest *pan*-inhibitory activity. Therefore, the development of Hsp90-isoform-selective inhibitors represents a novel opportunity for cancer treatment and provides a mechanism in which isoform-dependent substrates can be identified and ultimately targeted for degradation. While the on-target toxicities associated with *pan*-inhibition are poorly understood, they may be overcome via inhibition of individual Hsp90 isoforms. Thus, isoform-selective inhibitors such as those disclosed herein provide an opportunity to elucidate the individual roles played by each isoform and identify isoform-dependent substrates while evading the liabilities associated with *pan*-inhibition.

In an effort to develop new paradigms for Hsp90 inhibition, small molecule inhibitors that manifest selective inhibition of individual Hsp90 isoforms were pursued. Using a structure-based approach, a new series of rationally designed Hsp90β-selective inhibitors have now been disclosed. Analogues based on the benzamide inhibitor were developed and found to manifest Hsp90β-selective inhibition by taking advantage of minor structural differences that exist between the Hsp90α and Hsp90β N-terminal-binding sites, which until recently, was considered indistinguishable by ligands. Although only two amino acids differ within the binding sites of Hsp90α and Hsp90β, rationally designed analogues that perturb the conserved water molecules that reside in the subpocket led to the discovery of a novel scaffold that selectively inhibits the Hsp90β isoform. The reported isoquinolin-1(2*H*)-one series of compounds provides an improvement over the previously reported Hsp90β-selective inhibitor, **KUNB31**, by exhibiting an increase in affinity (~40−90 nM), selectivity (20 to >400-fold), and cellular efficacy.

Compound **4d** has been shown to manifest ~20-fold selectivity for Hsp90β, while compound **6a** manifests >45-fold selectivity for Hsp90β. Both **4d** and **6a** demonstrate selectivity toward specific cancer cell lines. In fact, **4d** was screened against the NCI-60 cancer cell panel to identify cancer cell lines sensitive to Hsp90β inhibition. Several cancers were inhibited by **4d** at low nanomolar concentrations and at concentrations comparable to the *pan*-inhibitors that have undergone clinical evaluation. Furthermore, Hsp90β-selective inhibition via **4d** and **6a** induced the degradation of Hsp90β-dependent clients, further supporting isoform inhibition as a distinct and alternative mechanism for the treatment of cancer.

In conclusion, a potent Hsp90β-selective series has been described that provides the opportunity to evade the detriments associated with Hsp90 *pan*-inhibition.

EXPERIMENTAL SECTION

General Information. All reactions were performed in oven-dried glassware under an argon atmosphere unless otherwise stated. Commercially available anhydrous solvents and reagents were utilized during synthesis. Flash column chromatography was performed using silica gel (40−63 μm particle size). The 1H spectra were recorded on a Brucker instrument at 600, 500, and 400 MHz frequencies and ^{13}C NMR were recorded at 151, 126, and 101 MHz frequencies. Data are reported as p = pentet, q = quartet, t = triplet, d = doublet, s = singlet, bs = broad singlet, m = multiplet; coupling constant(s) in Hz. High-resolution mass spectral data were obtained on a time-of-flight mass spectrometer, and analysis was performed using electrospray ionization. The final products were determined to be ≥95% purity using an Agilent technologies Infinity II instrument with a Poroshell 120 EC-C18 2.7 μm (4.6 × 100 mm) column using a solvent gradient of solvent A (H_2O with 0.1% trifluoroacetic acid) and solvent B (acetonitrile with 0.1% trifluoroacetic acid). Thin-layer chromatography was performed with TLC Sslica gel 60F254 plates purchased from Millipore Sigma and visualized by UV light.

*2,6-Difluoro-4-(3,6,6-trimethyl-4-oxo-4,5,6,7-tetrahydro-1H-indazol-1-yl)benzonitrile (**2**).*

(a) To a solution of 2,4,6-trifluurobenzonitrile (**1**) (5 g, 31.8 mmol, 1 equiv) in 50 mL of ethanol heated to 60 °C was added hydrazine hydrate (50−60% solution) (3.4 g, 63.6 mmol, ~2 equiv). Upon consumption of **1** (monitored using TLC), the solvent was evaporated from the reaction mixture under vacuum. To the remaining white semisolid mass was added 50 mL water, and the organic mass was extracted with ethyl acetate (3 × 50 mL). The combined organic fractions were combined and washed with brine (100 mL). The organic fraction was separated and dried over sodium sulfate. Subsequently, evaporation of the organic layer provided ~6.5 g of the white mixture that was utilized in the next reaction without further purification.

(b) Above obtained crude product (6 g, 35.5 mmol, 1 equiv) was suspended in 100 mL ethanol in a 250 mL capacity sealed reaction vessel. 2-Acetyldimedone (16.1 g, 88.75 mmol, 2.5 equiv), an orange colored oil, was subsequently added to the reaction vessel, which was sealed and heated to 100 °C for 6 h. The reaction vessel was allowed to cool to rt, ethanol was removed in vacuo, and the remaining mass was extracted with ethyl acetate (3 × 100 mL) and water (200 mL). Organic layers were combined and washed with 100 mL of water. A separated organic layer was dried using sodium sulfate and adsorbed onto silica and purified using column chromatog-

https://dx.doi.org/10.1021/acs.jmedchem.0c01700
J. Med. Chem. 2021, 64, 1545−1557

raphy (SiO_2, 3:2 hexanes/ethyl acetate) to afford **2** (5.8 g, 52%) as light-yellow solid. ^{1}H NMR (500 MHz, chloroform-*d*) δ 7.39−7.33 (m, 2H), 2.91 (s, 2H), 2.55 (s, 3H), 2.45 (s, 2H), 1.17 (s, 6H). ^{13}C NMR (126 MHz, chloroform-*d*) δ 192.9, 164.5 (d, J = 6.5 Hz), 162.5 (d, J = 6.4 Hz), 151.8, 149.4, 144.5−144.1 (m), 118.8, 108.5, 106.2 (d, J = 4.1 Hz), 106.0 (d, J = 3.9 Hz), 99.9, 52.0, 38.0, 36.0, 28.4 (2), 13.3. HRMS (ESI) m/z [M + H] calcd for $C_{17}H_{16}F_2N_3O$, 316.1261, found 316.1237.

General Method for Preparation of ***3a−3i.***

(a) To a solution of benzonitrile **2** (200 mg, 0.64 mmol, 1 equiv) in 2 mL of DMF in a 10 mL round-bottom flask, desired β-ketoethylester (0.76 mmol, 1.2 equiv), potassium carbonate (106 mg, 0.76 mmol, 1.2 equiv) was added and stirred at 70 °C until **2** was consumed, as determined by TLC. Upon completion, the reaction was acidified to pH 5 with 1 N aq. HCl; subsequently, 10 mL of NH_4Cl saturated solution was added and extracted using ethyl acetate (3 × 10 mL). The combined organic fractions were washed with brine and dried over sodium sulfate. The organic fraction was then adsorbed on silica, and a quick flash column chromatography was performed using 3:7 ethyl acetate/hexane as the solvent system. The product fractions were collected and dried, and the resulting mass was utilized in the further reaction.

(b) The crude mass obtained (∼210 mg) was taken in a 15 mL sealed reaction vessel; to which, 1 mL of sulfuric acid (36 N) and 8.5 mL acetic acid and 0.5 mL water were added. The vessel was sealed and heated to 140 °C for 8 h. The reaction was then quenched with the addition of the reaction mixture to 100 mL of water. Precipitated solid was filtered under vacuum to yield a brown-colored solid cake that was dried, dissolved in ethyl acetate, and adsorbed onto silica for further purification. Upon column chromatography with 5:5 hexane/ethyl acetate, the desired product was isolated as white solid (30−40% yield).

8-Fluoro-3-methyl-6-(3,6,6-trimethyl-4-oxo-4,5,6,7-tetrahydro-1H-indazol-1-yl)isoquinolin-1(2H)-one ***(3a).*** Yield 35%, 78 mg; ^{1}H NMR (500 MHz, chloroform-*d*) δ 10.63 (s, 1H), 7.40−7.35 (m, 1H), 7.29−7.25 (m, 1H), 6.34 (s, 1H), 2.91 (s, 2H), 2.57 (s, 3H), 2.44 (s, 2H), 2.41 (d, J = 1.0 Hz, 3H), 1.15 (s, 6H). ^{13}C NMR (126 MHz, chloroform-*d*) δ 193.3, 163.0 (d, J = 265.2 Hz), 161.3 (d, J = 3.9 Hz), 150.8, 149.2, 142.4 (d, J = 11.7 Hz), 142.1 (d, J = 1.8 Hz), 140.5, 117.8, 114.3 (d, J = 4.2 Hz), 112.0 (d, J = 6.4 Hz), 107.5 (d, J = 25.6 Hz), 103.9 (d, J = 2.7 Hz), 52.2, 37.7, 36.0, 28.4 (2), 19.3, 13.4. HRMS (ESI) m/z [M + H] calcd for $C_{20}H_{20}FN_3O_2$, 354.1617, found 354.1626.

3-Ethyl-8-fluoro-6-(3,6,6-trimethyl-4-oxo-4,5,6,7-tetrahydro-1H-indazol-1-yl)isoquinolin-1(2H)-one ***(3b).*** Yield 36%, 77 mg; ^{1}H NMR (600 MHz, chloroform-*d*) δ 9.51 (s, 1H), 7.41 (d, J = 2.0 Hz, 1H), 7.27 (d, J = 0.6 Hz, 1H), 6.33 (s, 1H), 2.92 (s, 2H), 2.64 (q, J = 7.5 Hz, 2H), 2.57 (s, 3H), 2.44 (s, 2H), 1.36 (t, J = 7.5 Hz, 3H), 1.15 (s, 6H). ^{13}C NMR (151 MHz, chloroform-*d*) δ 193.3, 162.1, 160.8, 150.8, 149.2, 145.4, 142.5, 142.0, 117.9, 114.6 (d, J = 4.1 Hz), 112.3, 107.6 (d, J = 25.5 Hz), 102.8, 52.3, 37.7, 36.0, 28.4 (2), 26.4, 13.4, 12.0. HRMS (ESI) m/z [M + Na] calcd for $C_{21}H_{22}FN_3O_2Na$, 390.1594 found 390.1609.

8-Fluoro-3-isopropyl-6-(3,6,6-trimethyl-4-oxo-4,5,6,7-tetrahydro-1H-indazol-1-yl)isoquinolin-1(2H)-one ***(3c).*** Yield 40%, 96 mg; ^{1}H NMR (600 MHz, chloroform-*d*) δ 9.31 (s, 1H), 7.41 (d, J = 2.0 Hz, 1H), 7.27 (dd, J = 11.7, 2.0 Hz, 1H), 6.32 (s, 1H), 2.91 (s, 2H), 2.86−2.79 (m, 1H), 2.57 (s, 3H), 2.44 (s, 2H), 1.36 (d, J = 6.9 Hz, 6H), 1.15 (s, 6H). ^{13}C NMR (151 MHz, chloroform-*d*) δ 193.31, 162.99 (d, J = 265.3 Hz), 160.6, 150.8, 149.4, 149.2, 142.4 (d, J = 11.7 Hz), 142.0, 117.9, 114.8 (d, J = 4.3 Hz), 112.4, 107.6 (d, J = 25.6 Hz), 100.9 (d, J = 2.6 Hz), 52.3, 37.7, 36.0, 32.2, 28.4 (2), 21.2 (2), 13.4. HRMS (ESI) m/z [M + Na] calcd for $C_{22}H_{24}FN_3O_2Na$, 404.1750, found 404.1743.

8-Fluoro-3-propyl-6-(3,6,6-trimethyl-4-oxo-4,5,6,7-tetrahydro-1H-indazol-1-yl)isoquinolin-1(2H)-one ***(3d).*** Yield 45%, 113 mg; ^{1}H NMR (500 MHz, chloroform-*d*) δ 10.32 (s, 1H), 7.40 (d, J = 2.0 Hz, 1H), 7.26 (d, J = 14.0 Hz, 1H), 6.37−6.29 (s, 1H), 2.91 (s, 2H), 2.61 (t, J = 7.6 Hz, 2H), 2.57 (s, 3H), 2.44 (s, 2H), 1.80 (h, J = 7.4 Hz, 2H), 1.15 (s, 6H), 1.04 (t, J = 7.4 Hz, 3H). ^{13}C NMR (126 MHz, chloroform-*d*) δ 193.3, 162.9 (d, J = 265.2 Hz), 161.1 (d, J = 4.5 Hz), 150.8, 149.3, 144.5, 142.8 (d, J = 11.9 Hz), 142.0 (d, J = 2.4 Hz), 117.8, 114.6 (d, J = 4.6 Hz), 112.2 (d, J = 7.2 Hz), 107.5 (d, J = 25.7 Hz), 103.3 (d, J = 3.5 Hz), 52.3, 37.8, 36.0, 35.2, 28.4 (2), 21.4, 13.5, 13.4. HRMS (ESI) m/z [M + Na] calcd for $C_{22}H_{24}FN_3O_2Na$, 404.1750, found 404.1765.

3-Butyl-8-fluoro-6-(3,6,6-trimethyl-4-oxo-4,5,6,7-tetrahydro-1H-indazol-1-yl)isoquinolin-1(2H)-one ***(3e).*** Yield 40%, 100 mg; ^{1}H NMR (600 MHz, chloroform-*d*) δ 9.99 (d, J = 20.1 Hz, 1H), 7.40 (d, J = 1.9 Hz, 1H), 7.25 (dd, J = 11.6, 2.0 Hz, 1H), 6.32 (s, 1H), 2.91 (s, 2H), 2.61 (t, J = 7.7 Hz, 2H), 2.58−2.55 (m, 3H), 2.44 (s, 2H), 1.73 (p, J = 7.7 Hz, 2H), 1.45 (h, J = 7.4 Hz, 2H), 1.15 (s, 6H), 1.01−0.95 (m, 3H). ^{13}C NMR (151 MHz, chloroform-*d*) δ 193.3, 163.0 (d, J = 265.5 Hz), 161.1 (d, J = 3.6 Hz), 150.8, 149.2, 144.6, 142.4 (d, J = 11.5 Hz), 142.1, 117.9, 114.6 (d, J = 4.1 Hz), 112.3 (d, J = 6.3 Hz), 107.5 (d, J = 25.5 Hz), 103.2 (d, J = 2.6 Hz), 52.3, 37.8, 36.0, 33.1, 30.1, 28.4 (2), 22.1, 13.7, 13.4. HRMS (ESI) m/z [M + Na] calcd for $C_{23}H_{26}FN_3O_2Na$, 418.1907, found 418.1902.

3-(tert-Butyl)-8-fluoro-6-(3,6,6-trimethyl-4-oxo-4,5,6,7-tetrahydro-1H-indazol-1-yl)isoquinolin-1(2H)-one ***(3f).*** Yield 38%, 95 mg; ^{1}H NMR (600 MHz, chloroform-*d*) δ 8.78 (s, 1H), 7.44 (d, J = 1.9 Hz, 1H), 7.27 (d, J = 0.7 Hz, 1H), 6.37 (s, 1H), 2.91 (s, 2H), 2.56 (s, 3H), 2.44 (s, 2H), 1.38 (s, 9H), 1.15 (s, 6H). ^{13}C NMR (151 MHz, chloroform-*d*) δ 193.3, 161.2 (d, J = 254.3 Hz), 155.6, 151.3, 150.8, 149.2, 142.4 (d, J = 11.5 Hz) 141.9, 140.8, 117.9, 115.1, 107.7 (d, J = 25.8 Hz), 100.3, 52.3, 37.8, 36.0, 34.5, 28.8 (3), 28.4 (2), 13.4. HRMS (ESI) m/z [M + Na] calcd for $C_{23}H_{26}FN_3O_2Na$, 418.1907, found 418.1897.

8-Fluoro-3-isobutyl-6-(3,6,6-trimethyl-4-oxo-4,5,6,7-tetrahydro-1H-indazol-1-yl)isoquinolin-1(2H)-one ***(3g).*** Yield 35%, 88 mg; ^{1}H NMR (600 MHz, chloroform-*d*) δ 8.74 (s, 1H), 7.43 (d, J = 2.0 Hz, 1H), 7.24 (dd, J = 11.7, 2.0 Hz, 1H), 6.28 (s, 1H), 2.91 (s, 2H), 2.56 (s, 3H), 2.44 (s, 2H), 2.41 (d, J = 7.4 Hz, 2H), 1.15 (s, 6H), 1.02 (d, J = 6.6 Hz, 6H). ^{13}C NMR (151 MHz, chloroform-*d*) δ 197.0, 171.0, 161.3 (d, J = 3.9 Hz), 150.8, 149.2, 148.7, 142.5 (d, J = 11.7 Hz), 142.1 (d, J = 1.8 Hz), 139.2, 122.4, 114.3 (d, J = 4.2 Hz), 112.0 (d, J = 6.4 Hz), 107.5 (d, J = 25.6 Hz), 103.9 (d, J = 2.7 Hz), 53.4, 42.8, 37.7, 36.0, 28.4, 22.2 (2), 14.2 (2). HRMS (ESI) m/z [M + Na] calcd for $C_{23}H_{26}FN_3O_2Na$, 418.1907, found 418.1913.

3-Cyclopropyl-8-fluoro-6-(3,6,6-trimethyl-4-oxo-4,5,6,7-tetrahydro-1H-indazol-1-yl)isoquinolin-1(2H)-one ***(3h).*** Yield 33%, 80 mg; ^{1}H NMR (600 MHz, chloroform-*d*) δ 9.43 (s, 1H), 7.38−7.35 (m, 1H), 7.23 (dd, J = 11.8, 2.0 Hz, 1H), 6.24−6.20 (m, 1H), 2.90 (s, 2H), 2.56 (s, 3H), 2.43 (s, 2H), 1.90−1.83 (m, 1H), 1.14 (s, 6H), 1.10−1.08 (m, 2H), 0.93−0.90 (m, 2H). ^{13}C NMR (151 MHz, chloroform-*d*) δ 193.3, 163.0 (d, J = 265.1 Hz), 160.6, 150.8, 149.2, 145.7, 142.5, 142.0, 117.9, 114.4 (d, J = 4.2 Hz), 112.2 (d, J = 6.3 Hz), 107.4 (d, J = 25.5 Hz), 101.1 (d, J = 2.7 Hz), 52.3, 37.8, 35.9, 28.4 (2), 13.5, 13.4, 7.4 (2). HRMS (ESI) m/z [M + Na] calcd for $C_{22}H_{22}FN_3O_2Na$, 402.1594, found 402.1603.

8-Fluoro-3-(methoxymethyl)-6-(3,6,6-trimethyl-4-oxo-4,5,6,7-tetrahydro-1H-indazol-1-yl)isoquinolin-1(2H)-one ***(3i).*** Yield 33%, 80 mg; ^{1}H NMR (600 MHz, chloroform-*d*) δ 8.74 (s, 1H), 7.38 (d, J = 2.0 Hz, 1H), 7.22 (dd, J = 11.7, 2.0 Hz, 1H), 6.30 (s, 1H), 4.30 (s, 2H), 3.39 (s, 3H), 2.83 (s, 2H), 2.49 (s, 3H), 2.36 (s, 2H), 1.07 (s, 6H). ^{13}C NMR (126 MHz, chloroform-*d*) δ 193.2, 162.9 (d, J = 265.1 Hz), 159.7, 150.9, 149.2, 142.6, 141.2 (d, J = 2.2 Hz), 139.5, 117.9, 114.9 (d, J = 4.6 Hz), 113.3 (d, J = 6.2 Hz), 108.2 (d, J = 25.7 Hz), 102.6 (d, J = 3.3 Hz), 70.0, 58.7, 52.2 37.8, 35.9, 28.4 (2), 13.4. HRMS (ESI) m/z [M + H] calcd for $C_{21}H_{23}FN_3O_3$, 384.1723, found 384.1716.

8-Fluoro-3-(hydroxymethyl)-6-(3,6,6-trimethyl-4-oxo-4,5,6,7-tetrahydro-1H-indazol-1-yl)isoquinolin-1(2H)-one ***(3j).*** To a solution of **3i** (100 mg, 0.26 mmol, 1 equiv) in 3 mL of DCM cooled to 0 °C was added 0.8 mL of 1 M BBr_3 solution in DCM (0.78 mmol, 3 equiv) dropwise, the reaction completion was monitored using TLC.

https://dx.doi.org/10.1021/acs.jmedchem.0c01700
J. Med. Chem. 2021, 64, 1545−1557

After 2 h, the reaction was quenched dropwise using 2 mL of saturated sodium bicarbonate solution, and resulting biphasic mixture was extracted using ethyl acetate (10 mL × 2). The organic fractions were collected, washed with water, and dried over sodium sulfate. The organic fraction was adsorbed onto silica for column chromatography purification using (4:6 ethyl acetate/hexane) to furnish 55 mg (0.155 mmol, yield 60%) as white solid. ^{1}H NMR (600 MHz, chloroform-*d*) δ 10.28 (s, 1H), 7.35 (d, J = 1.9 Hz, 1H), 7.24 (dd, J = 11.8, 2.0 Hz, 1H), 6.36 (s, 1H), 4.59 (s, 2H), 2.83 (s, 2H), 2.49 (s, 3H), 2.36 (s, 2H), 1.07 (s, 6H). ^{13}C NMR (126 MHz, chloroform-*d*) δ 193.25, 166.29 (d, J = 265.1 Hz) 151.0, 149.3, 142.3, 141.4, 118.0, 114.9 (d, J = 4.6 Hz), 112.7, 108.2 (d, J = 25.4 Hz), 102.7 (d, J = 2.9 Hz), 100.8, 99.9, 61.1, 52.2, 37.7, 35.9, 28.4 (2), 13.4. HRMS (ESI) m/z [M + H] calcd for $C_{20}H_{21}FN_3O_3$, 370.1567, found 370.1581.

General Procedure for Preparation of ***4a*****–*****5j*** *and* ***5a*****–*****5g***. A solution of the desired intermediate **3a**–**3j** (0.07 mmol, 1 equiv) in 1 mL of DMSO was taken in a 5 mL sealed reaction vessel; the corresponding amine (*trans*-4-aminocyclohexanol for **4a**–**4j**) (0.212 mmol, 3 equiv) and then diisopropyl ethyl amine (DIPEA)(0.212 mmol, 3 equiv) were introduced. The reaction vessel was then sealed and heated to 140 °C for 12 h and cooled, and water (25 mL) was added. The aqueous layer was extracted with ethyl acetate (25 mL × 3); the organic fractions were combined and washed with brine (25 mL) and dried over sodium sulfate. Purification with column chromatography (SiO_2, 4:96 methanol/DCM for **4a**–**4k**, **5a**, **5b**, **5e** and 5:1:94 methanol:7 M NH_3 in methanol/DCM for **5c**, **5d**, **5f**, and **5 g**) resulted in the desired products, which were further purified by preparative TLC to give the desired compounds **4a**–**4j** and **5a**–**5g** as light yellow solids.

8-(((1r,4r)-4-Hydroxycyclohexyl)amino)-3-methyl-6-(3,6,6-trimethyl-4-oxo-4,5,6,7-tetrahydro-1H-indazol-1-yl)isoquinolin-1(2H)-one ***(4a)***. Yield 70%, 22 mg; ^{1}H NMR (400 MHz, chloroform-*d*) δ 9.16 (d, J = 7.5 Hz, 1H), 9.05 (s, 1H), 6.51–6.40 (m, 2H), 6.09 (s, 1H), 3.74–3.59 (m, 2H), 3.31 (d, J = 24.2 Hz, 1H), 2.78 (s, 2H), 2.49 (s, 3H), 2.34 (s, 2H), 2.19 (s, 3H), 2.17–2.08 (m, 2H), 2.04–1.95 (m, 2H), 1.38 (q, J = 11.1, 9.9 Hz, 4H), 1.04 (s, 6H). ^{13}C NMR (101 MHz, $CDCl_3$) δ 193.4, 185.3, 169.7, 165.5, 151.4, 150.0, 149.1, 143.5, 143.2, 142.1, 137.4, 107.3, 105.7, 104.8, 100.3, 69.7, 52.4, 50.2, 37.8, 35.8, 33.5, 29.9, 28.4 (2), 19.0, 13.4. HRMS (ESI) m/z [M + H] calcd for $C_{26}H_{33}N_4O_3$, 449.2553, found 449.2566.

3-Ethyl-8-(((1r,4r)-4-hydroxycyclohexyl)amino)-6-(3,6,6-trimethyl-4-oxo-4,5,6,7-tetrahydro-1H-indazol-1-yl)isoquinolin-1(2H)-one ***(4b)***. Yield 58%, 19 mg; ^{1}H NMR (500 MHz, chloroform-*d*) δ 9.77 (s, 1H), 9.45 (s, 1H), 6.63 (d, J = 2.0 Hz, 1H), 6.56 (d, J = 1.9 Hz, 1H), 6.26–6.16 (m, 1H), 3.77 (dd, J = 8.7, 4.4 Hz, 1H), 3.44 (s, 1H), 2.89 (s, 2H), 2.62–2.55 (m, 5H), 2.43 (s, 2H), 2.30–2.17 (m, 2H), 2.10 (d, J = 10.4 Hz, 3H), 1.54–1.42 (m, 4H), 1.32 (q, J = 7.6 Hz, 3H), 1.14 (s, 6H). ^{13}C NMR (126 MHz, $CDCl_3$) δ 193.4, 165.6, 150.9, 150.1, 149.5, 149.1, 143.4, 143.1, 142.1, 119.4, 117.3, 104.3, 99.9, 88.4, 69.6, 52.4, 37.8, 35.8 (2), 33.5 (2), 29.7, 29.7, 28.4 (2), 26.1, 13.5, 12.4. HRMS (ESI) m/z [M + H] calcd for $C_{28}H_{38}N_5O_2$, 476.3026, found 476.3049.

8-(((1r,4r)-4-Hydroxycyclohexyl)amino)-3-isopropyl-6-(3,6,6-trimethyl-4-oxo-4,5,6,7-tetrahydro-1H-indazol-1-yl)isoquinolin-1(2H)-one ***(4c)***. Yield 65%, 21 mg; ^{1}H NMR (500 MHz, chloroform-*d*) δ 11.01–10.60 (m, 1H), 9.29 (d, J = 7.4 Hz, 1H), 6.59 (d, J = 2.0 Hz, 1H), 6.52 (d, J = 1.9 Hz, 1H), 6.21 (d, J = 1.8 Hz, 1H), 3.79–3.70 (m, 1H), 3.47–3.38 (m, 1H), 2.88–2.77 (m, 3H), 2.56 (s, 3H), 2.41 (s, 2H), 2.25–2.18 (m, 2H), 2.10–2.04 (m, 2H), 1.52–1.38 (m, 4H), 1.34 (d, J = 6.9 Hz, 6H), 1.11 (s, 6H). ^{13}C NMR (126 MHz, chloroform-*d*) δ 193.6, 166.8–165.9 (m), 151.3 (d, J = 15.4 Hz), 149.9, 149.2, 147.6 (d, J = 17.2 Hz), 143.1, 142.2, 117.1, 107.6 (d, J = 2.7 Hz), 105.1 (d, J = 2.7 Hz), 102.9 (t, J = 2.6 Hz), 100.1, 69.7, 52.4, 50.1 (d, J = 11.0 Hz), 37.7, 35.9, 33.6 (2), 31.9 (d, J = 6.7 Hz), 30.2 (2), 28.4 (2), 21.4 (2), 13.48. HRMS (ESI) m/z [M + Na] calcd for $C_{28}H_{37}N_4O_3Na$, 499.2685, found 499.2672.

8-(((1r,4r)-4-Hydroxycyclohexyl)amino)-3-propyl-6-(3,6,6-trimethyl-4-oxo-4,5,6,7-tetrahydro-1H-indazol-1-yl)isoquinolin-1(2H)-one ***(4d)***. Yield 65%, 22 mg; ^{1}H NMR (500 MHz, chloroform-*d*) δ 10.44 (s, 1H), 9.29 (d, J = 7.4 Hz, 1H), 6.60 (d, J = 1.9 Hz, 1H), 6.51 (d, J = 1.9 Hz, 1H), 6.21 (d, J = 1.9 Hz, 1H), 3.80–3.73 (m, 1H), 3.47–3.38 (m, 1H), 2.87 (s, 2H), 2.58 (s, 3H), 2.54 (t, J = 7.5 Hz, 2H), 2.43 (s, 2H), 2.28–2.20 (m, 2H), 2.12–2.03 (m, 2H), 1.76 (h, J = 7.4 Hz, 2H), 1.55–1.36 (m, 4H), 1.13 (s, 6H), 1.01 (t, J = 7.3 Hz, 3H). ^{13}C NMR (126 MHz, chloroform-*d*) δ 193.5, 166.3, 151.4, 149.9, 149.1, 143.1, 142.2, 141.9, 117.2, 107.5, 105.4, 104.9, 100.0, 69.8, 52.4, 50.2, 37.7, 35.9, 34.8, 33.6 (2), 30.1 (2), 28.4 (2), 21.3, 13.5, 13.5. HRMS (ESI) m/z [M + Na] calcd for $C_{28}H_{36}N_4O_3Na$, 499.2685, found 499.2688.

3-Butyl-8-(((1r,4r)-4-hydroxycyclohexyl)amino)-6-(3,6,6-trimethyl-4-oxo-4,5,6,7-tetrahydro-1H-indazol-1-yl)isoquinolin-1(2H)-one ***(4e)***. Yield 58%, 20 mg; ^{1}H NMR (500 MHz, chloroform-*d*) δ 10.21 (s, 1H), 9.27 (d, J = 7.5 Hz, 1H), 6.59 (d, J = 1.9 Hz, 1H), 6.51 (d, J = 2.0 Hz, 1H), 6.20 (d, J = 2.0 Hz, 1H), 3.79–3.72 (m, 1H), 3.47–3.37 (m, 1H), 2.87 (s, 2H), 2.60–2.52 (m, 5H), 2.42 (s, 2H), 2.26–2.19 (m, 2H), 2.11–2.05 (m, 2H), 1.74–1.64 (m, 2H), 1.54–1.32 (m, 6H), 1.12 (s, 6H), 0.96 (t, J = 7.3 Hz, 3H). ^{13}C NMR (126 MHz, chloroform-*d*) δ 193.5, 166.1, 151.4, 149.9, 149.1, 143.1, 142.2, 142.1, 117.2, 107.5, 105.2, 104.9, 100.1, 69.8, 52.4, 50.2, 37.7, 35.8, 33.7 (2), 32.6, 30.1 (2), 30.0, 28.4 (2), 22.1, 13.9, 13.5. HRMS (ESI) m/z [M + H] calcd for $C_{29}H_{39}N_4O_3$, 491.3022, found 491.3011.

3-(tert-Butyl)-8-(((1r,4r)-4-hydroxycyclohexyl)amino)-6-(3,6,6-trimethyl-4-oxo-4,5,6,7-tetrahydro-1H-indazol-1-yl)isoquinolin-1(2H)-one ***(4f)***. Yield 65%, 22 mg; ^{1}H NMR (500 MHz, chloroform-*d*) δ 9.53 (s, 1H), 9.28 (d, J = 6.9 Hz, 1H), 6.68–6.51 (m, 2H), 6.27 (d, J = 2.1 Hz, 1H), 3.80–3.73 (m, 1H), 3.47–3.43 (m, 1H), 2.88 (s, 2H), 2.58 (s, 3H), 2.43 (s, 2H), 2.25–2.18 (m, 2H), 2.13–2.06 (m, 2H), 1.53–1.40 (m, 4H), 1.38 (s, 9H), 1.13 (s, 6H). ^{13}C NMR (126 MHz, chloroform-*d*) δ 193.5, 165.7, 150.9, 150.0, 149.3, 149.1, 143.2, 141.9, 117.2, 107.6, 105.8, 102.3, 100.7, 69.8, 52.4, 50.6, 37.8, 35.9, 34.3, 33.7 (2), 30.1 (2), 28.9 (3), 28.4 (2), 13.5. HRMS (ESI) m/z [M + Na] calcd for $C_{29}H_{38}N_4O_3Na$, 513.2842, found 513.2821.

8-(((1r,4r)-4-Hydroxycyclohexyl)amino)-3-isobutyl-6-(3,6,6-trimethyl-4-oxo-4,5,6,7-tetrahydro-1H-indazol-1-yl)isoquinolin-1(2H)-one ***(4g)***. Yield 55%, 19 mg; ^{1}H NMR (500 MHz, chloroform-*d*) δ 9.57 (s, 1H), 9.24 (d, J = 7.5 Hz, 1H), 6.60 (d, J = 1.9 Hz, 1H), 6.50 (d, J = 1.9 Hz, 1H), 6.17 (d, J = 2.0 Hz, 1H), 3.80–3.72 (m, 1H), 3.46–3.37 (m, 1H), 2.87 (s, 2H), 2.63 (s, 4H), 2.42 (s, 2H), 2.39 (d, J = 7.4 Hz, 2H), 2.23 (dd, J = 9.4, 5.0 Hz, 2H), 2.11–1.97 (m, 3H), 1.53–1.39 (m, 4H), 1.12 (s, 6H), 0.99 (d, J = 6.6 Hz, 6H). ^{13}C NMR (126 MHz, chloroform-*d*) δ 193.5, 165.9, 151.4, 150.0, 149.1, 143.1, 142.0, 141.0, 117.2, 107.5, 106.1, 105.0, 100.1, 69.8, 52.4, 50.3, 42.4, 37.7, 35.8, 33.7 (2), 30.1 (2), 28.4, 27.9 (2), 22.3 (2), 13.5. HRMS (ESI) m/z [M + H] calcd for $C_{29}H_{39}N_4O_3$, 491.3022, found 491.3019.

3-Cyclopropyl-8-(((1r,4r)-4-hydroxycyclohexyl)amino)-6-(3,6,6-trimethyl-4-oxo-4,5,6,7-tetrahydro-1H-indazol-1-yl)isoquinolin-1(2H)-one ***(4h)***. Yield 66%, 22 mg; ^{1}H NMR (500 MHz, chloroform-*d*) δ 9.67 (s, 1H), 9.26 (d, J = 7.2 Hz, 1H), 6.58 (d, J = 1.9 Hz, 1H), 6.53 (d, J = 2.0 Hz, 1H), 6.15 (d, J = 1.9 Hz, 1H), 3.80–3.73 (m, 1H), 3.48–3.39 (m, 1H), 2.88 (s, 2H), 2.59 (s, 3H), 2.44 (s, 2H), 2.26–2.18 (m, 2H), 2.12–2.04 (m, 2H), 1.87–1.78 (m, 1H), 1.55–1.38 (m, 4H), 1.14 (s, 6H), 1.04–0.99 (m, 2H), 0.95–0.90 (m, 2H). ^{13}C NMR (126 MHz, chloroform-*d*) δ 193.5, 165.7, 150.0, 149.1, 143.2, 143.2, 142.0, 117.2, 107.5, 105.0, 103.4, 100.2, 69.8, 52.4, 50.3, 37.7, 35.8, 33.7 (2), 30.0 (2), 28.4 (2), 13.5, 13.4, 7.1 (2). HRMS (ESI) m/z [M + H] calcd for $C_{28}H_{35}N_4O_3$, 475.2709, found 475.2698.

8-(((1r,4r)-4-Hydroxycyclohexyl)amino)-3-(methoxymethyl)-6-(3,6,6-trimethyl-4-oxo-4,5,6,7-tetrahydro-1H-indazol-1-yl)-isoquinolin-1(2H)-one ***(4i)***. Yield 60%, 20 mg; ^{1}H NMR (400 MHz, chloroform-*d*) δ 9.27 (d, J = 7.5 Hz, 1H), 8.63 (s, 1H), 6.62 (d, J = 1.8 Hz, 1H), 6.56 (s, 1H), 6.25 (s, 1H), 4.32 (s, 2H), 3.42 (s, 3H), 2.86 (s, 2H), 2.57 (s, 3H), 2.42 (s, 2H), 2.21 (s, 2H), 2.07 (s, 2H), 1.49 (q, J = 11.9, 10.3 Hz, 4H), 1.12 (s, 6H). ^{13}C NMR (101 MHz, $CDCl_3$) δ 193.3, 164.9, 151.5, 150.0, 149.0, 143.2, 141.2, 137.1, 117.3, 108.4, 105.3, 105.1, 101.0, 70.2, 69.7, 58.4, 52.4, 50.3, 37.8, 35.8, 33.5 (2), 29.9 (2), 28.4 (2), 13.4. HRMS (ESI) m/z [M + H] calcd for $C_{27}H_{35}N_4O_4$, 479.2658, found 479.2665.

8-(((1r,4r)-4-Hydroxycyclohexyl)amino)-3-(hydroxymethyl)-6-(3,6,6-trimethyl-4-oxo-4,5,6,7-tetrahydro-1H-indazol-1-yl)-isoquinolin-1(2H)-one ***(4j)***. Yield 63%, 20 mg; ^{1}H NMR (400 MHz,

https://dx.doi.org/10.1021/acs.jmedchem.0c01700
J. Med. Chem. 2021, 64, 1545–1557

chloroform-*d*) δ 9.31 (s, 1H), 9.19 (d, *J* = 7.4 Hz, 1H), 6.55 (d, *J* = 1.7 Hz, 1H), 6.51 (d, *J* = 1.9 Hz, 1H), 6.22 (s, 1H), 4.49 (s, 2H), 3.79−3.64 (m, 1H), 3.40 (d, *J* = 16.0 Hz, 1H), 2.83 (s, 2H), 2.55 (s, 3H), 2.40 (s, 2H), 2.19 (d, *J* = 11.2 Hz, 2H), 2.09−2.00 (m, 2H), 1.44 (dd, *J* = 18.9, 9.5 Hz, 4H), 1.10 (s, 6H). ^{13}C NMR (101 MHz, $CDCl_3$) δ 193.6, 172.2, 151.4, 150.1, 149.3, 143.1, 141.5, 139.9, 117.2, 108.2, 105.4, 103.9, 100.8, 69.5, 60.7, 52.3, 50.2, 37.7, 35.8, 33.4 (2), 29.9 (2), 28.3 (2), 13.3. HRMS (ESI) *m/z* [M + H] calcd for $C_{26}H_{33}N_4O_4$, 465.2502, found 465.2501.

8-Morpholino-3-propyl-6-(3,6,6-trimethyl-4-oxo-4,5,6,7-tetrahydro-1H-indazol-1-yl)isoquinolin-1(2H)-one (**5a**). Yield 65%, 20 mg; ^{1}H NMR (400 MHz, chloroform-*d*) δ 9.53 (s, 1H), 7.10 (d, *J* = 2.0 Hz, 1H), 7.05 (d, *J* = 2.1 Hz, 1H), 6.25 (s, 1H), 4.00 (t, *J* = 4.5 Hz, 4H), 3.22 (s, 4H), 2.86 (s, 2H), 2.57 (s, 5H), 2.43 (s, 2H), 1.76 (h, *J* = 7.4 Hz, 2H), 1.12 (s, 6H), 1.03 (t, *J* = 7.3 Hz, 3H). ^{13}C NMR (126 MHz, $CDCl_3$) δ 193.4, 162.1, 155.4, 150.4, 149.1, 143.1, 142.8, 141.9, 117.5, 115.4, 112.9, 109.7, 104.3, 67.2 (2), 53.4 (2), 52.4, 37.6, 35.9, 34.8, 28.4 (2), 21.2, 13.5, 13.5. HRMS (ESI) *m/z* [M + H] calcd for $C_{26}H_{33}N_4O_3$, 449.2553, found 449.2557.

8-(4-Hydroxypiperidin-1-yl)-3-propyl-6-(3,6,6-trimethyl-4-oxo-4,5,6,7-tetrahydro-1H-indazol-1-yl)isoquinolin-1(2H)-one (**5b**). Yield 55%, 18 mg; ^{1}H NMR (500 MHz, chloroform-*d*) δ 9.03 (s, 1H), 6.98 (d, *J* = 3.3 Hz, 2H), 6.15 (s, 1H), 3.86 (s, 1H), 3.41 (s, 2H), 2.87 (s, 2H), 2.78 (s, 2H), 2.52−2.44 (m, 5H), 2.35 (s, 2H), 2.12−2.03 (m, 2H), 1.92−1.81 (m, 2H), 1.67 (h, *J* = 7.4 Hz, 2H), 1.05 (s, 6H), 0.95 (t, *J* = 7.4 Hz, 3H). ^{13}C NMR (126 MHz, $CDCl_3$) δ 193.5, 162.0, 155.8, 150.3, 149.1, 142.9, 142.4, 141.8, 117.4, 115.5, 112.4, 110.1, 104.2, 53.4, 52.4 (2), 37.6, 35.9, 34.9 (2), 30.9, 29.7, 28.4 (2), 21.1, 13.5, 13.5. HRMS (ESI) *m/z* [M + H] calcd for $C_{27}H_{35}N_4O_3$, 463.2709, found 463.2710.

8-(4-Methylpiperazin-1-yl)-3-propyl-6-(3,6,6-trimethyl-4-oxo-4,5,6,7-tetrahydro-1H-indazol-1-yl)isoquinolin-1(2H)-one (**5c**). Yield 55%, 18 mg; ^{1}H NMR (400 MHz, chloroform-*d*) δ 9.56 (s, 1H), 9.35 (d, *J* = 7.3 Hz, 1H), 7.17 (d, *J* = 2.0 Hz, 1H), 7.02 (d, *J* = 2.1 Hz, 1H), 6.19 (d, *J* = 1.9 Hz, 1H), 2.87 (s, 2H), 2.80 (s, 1H), 2.57 (s, 3H), 2.52 (t, *J* = 7.4 Hz, 2H), 2.43 (s, 2H), 2.33 (s, 3H), 2.26 (t, *J* = 10.5 Hz, 2H), 2.16−2.08 (m, 2H), 1.79−1.58 (m, 7H), 1.13 (s, 6H), 1.01 (t, *J* = 7.4 Hz, 3H). ^{13}C NMR (101 MHz, $CDCl_3$) δ 193.5, 165.8, 151.2, 149.9, 149.0, 143.1, 142.1, 141.6, 140.8, 107.7, 105.3, 105.0, 100.2, 52.4, 46.3, 37.7, 35.8, 34.9 (2), 32.1, 31.6, 31.4, 28.4 (2), 21.2 (2), 13.5, 13.4. HRMS (ESI) *m/z* [M + Na] calcd for $C_{28}H_{37}N_5O_2Na$, 498.2845, found 498.2823.

8-(Piperazin-1-yl)-3-propyl-6-(3,6,6-trimethyl-4-oxo-4,5,6,7-tetrahydro-1H-indazol-1-yl)isoquinolin-1(2H)-one (**5d**). Yield 45%, 14 mg; ^{1}H NMR (400 MHz, chloroform-*d*) δ 9.59 (s, 1H), 7.09 (d, *J* = 2.0 Hz, 1H), 7.04 (d, *J* = 2.0 Hz, 1H), 6.17 (s, 1H), 3.13 (s, 6H), 2.79 (s, 2H), 2.50 (s, 5H), 2.35 (s, 2H), 2.27−2.01 (m, 2H), 1.68 (h, *J* = 7.4 Hz, 2H), 1.05 (s, 6H), 0.95 (t, *J* = 7.3 Hz, 3H). ^{13}C NMR (126 MHz, $CDCl_3$) δ 193.4, 161.7, 155.8, 150.3, 149.1, 143.0, 142.2, 141.9, 117.4, 115.5, 112.7, 109.8, 104.3, 54.3, 52.4 (2), 46.1 (2), 37.6, 35.9, 34.9, 28.5 (2), 21.2, 13.5, 13.5. HRMS (ESI) *m/z* [M + H] calcd for $C_{26}H_{34}N_5O_2$, 448.2713, found 448.2706.

tert-Butyl-4-(1-oxo-3-propyl-6-(3,6,6-trimethyl-4-oxo-4,5,6,7-tetrahydro-1H-indazol-1-yl)-1,2-dihydroisoquinolin-8-yl)piperazine-1-carboxylate (**5e**). Yield 53%, 20 mg; ^{1}H NMR (500 MHz, chloroform-*d*) δ 8.93 (s, 1H), 7.01 (d, *J* = 2.0 Hz, 1H), 6.96 (d, *J* = 2.1 Hz, 1H), 6.16 (d, *J* = 2.0 Hz, 1H), 3.75 (s, 4H), 3.08 (s, 4H), 2.79 (s, 2H), 2.51−2.43 (m, 5H), 2.35 (s, 2H), 1.66 (h, *J* = 7.4 Hz, 2H), 1.42 (s, 9H), 1.05 (s, 6H), 0.94 (t, *J* = 7.3 Hz, 3H). ^{13}C NMR (126 MHz, $CDCl_3$) δ 193.4, 161.8, 155.4, 154.9, 150.4, 149.1, 143.0, 142.5, 141.9, 117.5, 115.6, 112.9, 110.0, 104.2, 79.8, 53.0 (2), 52.4 (2), 37.6, 35.9, 34.9, 31.6, 28.5 (4), 21.1, 13.5, 13.5. HRMS (ESI) *m/z* [M + H] calcd for $C_{31}H_{42}N_5O_4$, 548.3237, found 548.3226.

8-((1-Methylpiperidin-4-yl)amino)-3-propyl-6-(3,6,6-trimethyl-4-oxo-4,5,6,7-tetrahydro-1H-indazol-1-yl)isoquinolin-1(2H)-one (**5f**). Yield 40%, 13 mg; ^{1}H NMR (400 MHz, chloroform-*d*) δ 9.56 (s, 1H), 9.35 (d, *J* = 7.3 Hz, 1H), 6.60 (d, *J* = 2.0 Hz, 1H), 6.53 (d, *J* = 2.1 Hz, 1H), 6.19 (d, *J* = 1.9 Hz, 1H), 2.87 (s, 2H), 2.80 (s, 1H), 2.57 (s, 3H), 2.52 (t, *J* = 7.4 Hz, 2H), 2.43 (s, 2H), 2.33 (s, 3H), 2.26 (t, *J* = 10.5 Hz, 2H), 2.16−2.08 (m, 2H), 1.79−1.58 (m, 7H), 1.13 (s, 6H), 1.01 (t, *J* = 7.4 Hz, 3H). ^{13}C NMR (101 MHz, $CDCl_3$) δ 193.5, 165.8, 151.3, 149.9, 149.1, 143.1, 142.1, 141.6, 140.8, 107.6, 105.3, 105.0, 100.2, 52.4, 46.3, 37.7, 35.8, 34.9 (2), 32.1, 31.6, 31.4, 28.4 (2), 21.2 (2), 13.5, 13.4. HRMS (ESI) *m/z* [M + Na] calcd for $C_{28}H_{37}N_5O_2Na$, 498.2845, found 498.2823.

8-((2-(Diethylamino)ethyl)(methyl)amino)-3-propyl-6-(3,6,6-trimethyl-4-oxo-4,5,6,7-tetrahydro-1H-indazol-1-yl)isoquinolin-1(2H)-one (**5g**). Yield 45%, 14 mg; ^{1}H NMR (500 MHz, chloroform-*d*) δ 9.22 (s, 1H), 7.03 (d, *J* = 2.0 Hz, 1H), 7.00 (d, *J* = 2.0 Hz, 1H), 6.21 (s, 1H), 3.44−3.37 (m, 2H), 3.02 (s, 3H), 2.86 (s, 2H), 2.77 (t, *J* = 7.4 Hz, 2H), 2.57 (s, 3H), 2.56−2.48 (m, 6H), 2.42 (s, 2H), 1.81−1.71 (m, 2H), 1.12 (s, 6H), 1.03 (t, *J* = 7.3 Hz, 3H), 0.97 (t, *J* = 7.1 Hz, 6H). ^{13}C NMR (126 MHz, $CDCl_3$) δ 193.5, 162.0, 155.2, 150.1, 149.1, 142.9, 141.5, 117.3, 114.5, 111.4, 110.0, 104.3, 55.5, 52.4, 50.4, 47.3 (2), 41.7, 37.5, 35.9, 35.0, 29.9, 28.4 (2), 21.2, 13.6, 13.5 (2), 11.7. HRMS (ESI) *m/z* [M + H] calcd for $C_{29}H_{42}N_5O_2$, 492.3338, found 492.3352.

General Procedure for the Syntheses of 6a and 6b. To a solution of **4d**/**5b** (0.1 mmol, 1 equiv) in 10 mL of ethanol was introduced palladium (10% on activated carbon) (10 mol %) in a pressure reactor vessel. After multiple cycles of degassing under vacuum, hydrogen gas was introduced at 200 psi and the reactor vessel was heated to 90 °C for 24 h. Upon completion, the reaction mixture was passed through a plug of Celite and solvent was removed under vacuum. Subsequently, preparative TLC was performed (SiO_2, 5% MeOH in dichloromethane) to obtain the desired compounds.

8-(((1r,4r)-4-Hydroxycyclohexyl)amino)-3-propyl-6-(3,6,6-trimethyl-4-oxo-4,5,6,7-tetrahydro-1H-indazol-1-yl)-3,4-dihydroisoquinolin-1(2H)-one (**6a**). White amorphous solid, 20 mg, yield 42%. ^{1}H NMR (400 MHz, chloroform-*d*) δ 8.78 (d, *J* = 7.5 Hz, 1H), 6.56 (d, *J* = 2.0 Hz, 1H), 6.49 (d, *J* = 1.9 Hz, 1H), 5.72 (s, 1H), 3.75 (dt, *J* = 9.6, 4.9 Hz, 1H), 3.60 (m, *J* = 8.4, 6.8, 5.0, 2.7 Hz, 1H), 3.40−3.27 (m, 1H), 2.91 (dd, *J* = 15.4, 4.2 Hz, 1H), 2.83 (s, 2H), 2.74 (dd, *J* = 15.3, 10.5 Hz, 1H), 2.55 (s, 3H), 2.41 (s, 2H), 2.23−1.98 (m, 4H), 1.64−1.52 (m, 2H), 1.50−1.36 (m, 6H), 1.12 (s, 6H), 0.97 (t, *J* = 7.2 Hz, 3H). ^{13}C NMR (101 MHz, $CDCl_3$) δ 193.4, 168.7, 150.7, 150.0, 148.9, 142.3, 142.0, 117.2, 108.5, 107.9, 104.1, 69.6, 53.4, 52.3, 50.5, 50.2, 37.7, 37.2, 35.8, 35.6, 33.6, 30.2, 30.1 (2), 28.4, 18.6, 13.9, 13.4. HRMS (ESI) *m/z* [M + H] calcd for $C_{28}H_{39}N_4O_3$, 479.3017, found 479.3041.

8-(4-Hydroxypiperidin-1-yl)-3-propyl-6-(3,6,6-trimethyl-4-oxo-4,5,6,7-tetrahydro-1H-indazol-1-yl)-3,4-dihydroisoquinolin-1(2H)-one (**6b**). White amorphous solid, 24 mg, yield 47%; ^{1}H NMR (400 MHz, chloroform-*d*) δ 6.94 (d, *J* = 2.1 Hz, 1H), 6.85 (d, *J* = 2.1 Hz, 1H), 6.01−5.90 (m, 1H), 3.88 (dd, *J* = 8.5, 4.6 Hz, 1H), 3.66−3.54 (m, *J* = 10.5, 6.6, 3.2 Hz, 1H), 3.50−3.32 (m, 3H), 3.05−2.88 (m, 3H), 2.82−2.71 (m, 3H), 2.54 (s, 3H), 2.42−2.36 (m, 2H), 2.16−1.98 (m, 1H), 1.99−1.74 (m, 2H), 1.65−1.52 (m, 2H), 1.51−1.37 (m, *J* = 14.3, 7.2, 5.1 Hz, 2H), 1.10 (d, *J* = 6.6 Hz, 6H), 0.97 (t, *J* = 7.2 Hz, 3H). ^{13}C NMR (101 MHz, $CDCl_3$) δ 193.4, 165.2, 153.8, 150.1, 149.0, 143.0, 141.1, 118.1, 117.2, 114.0, 111.8, 67.4, 52.3, 50.2, 50.1, 49.5, 37.4, 36.9, 36.8, 35.9, 34.3, 34.2, 28.5, 28.3, 18.8, 13.9, 13.4. HRMS (ESI) *m/z* [M + H] calcd for $C_{27}H_{37}N_4O_3$, 465.2860, found 465.2864.

Fluorescence Polarization Assay. The assay was performed in a 96-well format in black, flat-bottom plates (Santa Cruz Biotechnology) with a final volume of 100 μL. Twenty-five microliters of assay buffer (20 mM HEPES, pH 7.3, 50 mM KCl, 5 mM MgCl2, 20 mM Na2MoO4, 2 mM DTT, 0.1 mg/mL BGG, and 0.01% NP-40), 25 μL of assay buffer containing 6 nM FITC-GDA (fluorescent tracer, stock in DMSO and diluted in assay buffer), and 50 μL of assay buffer containing 10 nM of Hsp90β(Enzo, ADI-SPP-777), Hsp90α(Enzo, ADI-SPP-776), Grp94(Enzo, ADI-SPP-766), or 50 nM Trap1 (Enzo, ADI-SPP-848) was added to each well. Compounds were tested in triplicate wells (1% DMSO final concentration). For each plate, wells containing buffer only (background), tracer in buffer only (low polarization control), and protein and tracer in buffer with 1% DMSO (high polarization control) were included. Plates were incubated at 4 °C with rocking for 2 h. Polarization values (in mP units) were measured at 37 °C with an excitation filter at 485 nm and an emission

https://dx.doi.org/10.1021/acs.jmedchem.0c01700
J. Med. Chem. 2021, 64, 1545−1557

filter at 528 nm. Polarization values were correlated to % tracer bound and compound concentrations. The concentration at which the tracer was 50% displaced by the inhibitor was determined using MS Excel and reported with a standard deviation value from average of triplicates.

Cell Proliferation Assay. Cell proliferation was measured by the Cell Titer-Glo luminescent cell viability assay (Promega, Madison, WI) according to the manufacturer's instructions. Bladder cancer cells/well (2 × 103) were cultured in 96-well white plates in media for 24 h and then treated by compounds for 72 h. Luminescent signals were read on the BioTek Synergy 4 plate reader (BioTek Instruments, Winooski, VT). Data were analyzed from three independent experiments performed in triplicate, and nonlinear regression and sigmoidal dose−response curves (GraphPad Prism, La Jolla, CA) were used to calculate IC_{50} and R^2 values.

Western Blot Analysis HCT-116 Cells. HCT-116 cells were grown in DMEM (Corning, 10-027-CV) containing 1% Pen-Strep (VWR, K952-100ML) and 10% FBS+ (Atlas Biologicals, F-0500-D),and plated in a 6-well plate (VWR, 10861−696). At ∼80%, cells were treated with GDA at 500 nM and compound **6a** at 100, 250, 1.25, and 2.5 μM for 24 h.

Cell culture samples were lysed using RIPA buffer-containing protease and phosphatase inhibitors. Lysate protein concentrations were determined by the BCA assay (Thermo). Samples were separated by SDS-PAGE using 4−20% SDS gradient gels (BioRad). Gel contents were transferred to PVDF membranes. Membranes were blocked with 7% nonfat dry milk solution. Blots were probed with antibodies raised against Erk5 (Cell Signaling, 3552S), CDK4, (Cell Signaling, 12790S), CDK6 (Cell Signaling, 3136S), beta-Actin (Cell Signaling, 3700S), Survivin (Cell Signaling, 2808S), and c-Raf (Cell Signaling, 7065S). Antibody dilutions were 1:1000 unless otherwise stated, and all secondary antibodies were used at 1:1000 (Southern Biotech). Blots were developed using ECL (Amersham, 45-000-999) on a ChemiDoc Imaging System (BioRad). Densitometry was performed using Image Lab software (BioRad).

Western Blot Analysis of Client Proteins in UMUC-3 Bladder Cancer Cells. After 24 h treatment of compounds, UMUC-3 cells were harvested. SDS-PAGE lysates were prepared in RIPA buffer with protease and phosphatase inhibitor cocktail (Sigma-Aldrich, Inc., St. Louis, MO) and lysed by three freeze−thaw cycles using liquid nitrogen and a 37 °C water bath. Protein concentration was determined using a DC protein assay (Bio-Rad Laboratories, Hercules, CA). Equal amounts of protein (20 μg) were loaded on a Novex E-PAGETM 8% protein gel (Life Technologies), transferred to a nitrocellulose membrane by Novex iBlotR Gel Transfer system (Invitrogen, Carlsbad, CA), blocked in protein-free (PBS) blocking buffer (Pierce, Thermo Scientific), and probed with primary antibodies (1:1000 dilution). Membranes were incubated with HRP conjugated secondary antibody (1:10:000 dilution) and visualized with the Odyssey Infrared Imager system (LI-COR, Lincoln, NE). All Western blots were probed for the loading control β-actin. The data were representative of at least three independent experiments.

siRNA Silencing of Hsp90α. siRNA-targeting HSP90α was obtained from Dharmacon (ON-TARGETplus SMARTpool, catalog no. L-005186−00-0005; ON-TARGETplus siRNA, catalog no. J-005186-08-0050). Negative control siRNA was obtained from Dharmacon (ON-TARGETplus control pool, catalog no. D-001810-10-05). SkBr3 cells were seeded in six-well plates at a density of 100,000 cells per well, 16 h before transfection. For each sample, siRNA was mixed with 100 mL of Opti-MEM (ThermoFisher Scientific) to a final concentration of 10 nM (mix A). In a separate tube, 5 mL of Lipofectamine RNAiMAX (Invitrogen) was mixed with 100 mL Opti-MEM (mix B). Mixes A and B were then combined and further incubated for 20 min at room temperature. The siRNA/Lipofectamine complexes were added dropwise to 3 mL of culture medium containing the cells. After 2.5 days, the culture medium containing siRNA/Lipofectamine complexes was removed, and fresh media containing indicated concentrations of KUNB106 or geldanamycin were added to the cells for 6 or 18 h. Cells were then lysed with TNES lysis buffer (50 mM Tris−HCl pH 7.5, 1% NP-40, 2 mM EDTA, and 100 mM NaCl) containing protease and phosphatase inhibitors (Sigma, catalog nos. 4693124001 and 4906845001, respectively). Total protein for each sample was determined by the BCA protein assay (ThermoFisher Scientific), and equal amounts of total protein were analyzed via Western blotting. Antibodies used included: anti-Hsp90a(D1A7, Cell Signaling, #8165); anti-ErbB2 (HER-2/c-erbB-2/neu Ab-17, ThermoFisher Scientific, #MS-730-P1-A); anti-phospho-Akt (Ser473, Cell Signaling, #9271); anti-Akt (Cell Signaling, #9272); anti-Cdk4 (H-22, Santa Cruz Biotechnology, #sc-601); anti-c-IAP1 (Cell Signaling, #4952); and anti-α-tubulin as a loading control (DM1A, EMD Millipore, #CP06).

Molecular Modeling. The Surflex−Docking module in SybylX was used for molecular modeling and docking studies. The co-crystal structures of SNX 2112 bound to Hsp90 (PDB code: 4NH7), compound 31 bound to Hsp90a (PDB code: 4O0B) and PU-3 bound to Hsp90b (PDB code:1UYM) were utilized for modeling experiments. Pymol was used for further visualization and figure preparation.

■ ASSOCIATED CONTENT

Supporting Information

The Supporting Information is available free of charge at https://pubs.acs.org/doi/10.1021/acs.jmedchem.0c01700.

Effect of Hsp90β inhibition on proliferation of Hsp90α KO cells, HPLC analysis of select compound, and NCI-60 cell line screening results of **4d** and **6a**; Grp94 and Trap1 inhibition data, GI50 values of **4a**, **5b**, and **6a** against Hek293 cells, molecular formula strings file with IC50 value against cancer cell lines and computational models (PDF)

Molecular formula strings (CSV)

4d (beta) (PDB)

4d (alpha) (PDB)

6a (beta) (PDB)

■ AUTHOR INFORMATION

Corresponding Author

Brian S. J. Blagg − *Department of Chemistry and Biochemistry, The University of Notre Dame, Notre Dame, Indiana 46556, United States;* orcid.org/0000-0002-6200-3480; Email: bblagg@nd.edu

Authors

Sanket J. Mishra − *Department of Chemistry and Biochemistry, The University of Notre Dame, Notre Dame, Indiana 46556, United States*

Weiya Liu − *Department of Urologic Oncology, University of Kansas Medical Center, Kansas City, Kansas 66160, United States*

Kristin Beebe − *Center for Cancer Research, National Cancer Institute, Rockville, Maryland 20892, United States*

Monimoy Banerjee − *Department of Chemistry and Biochemistry, The University of Notre Dame, Notre Dame, Indiana 46556, United States*

Caitlin N. Kent − *Department of Chemistry and Biochemistry, The University of Notre Dame, Notre Dame, Indiana 46556, United States*

Vitumbiko Munthali − *Department of Chemistry and Biochemistry, The University of Notre Dame, Notre Dame, Indiana 46556, United States*

John Koren, III − *Department of Chemistry and Biochemistry, The University of Notre Dame, Notre Dame, Indiana 46556, United States*

https://dx.doi.org/10.1021/acs.jmedchem.0c01700
J. Med. Chem. 2021, 64, 1545−1557

John A Taylor, III − *Department of Urologic Oncology, University of Kansas Medical Center, Kansas City, Kansas 66160, United States*
Leonard M. Neckers − *Center for Cancer Research, National Cancer Institute, Rockville, Maryland 20892, United States*
Jeffrey Holzbeierlein − *Department of Urologic Oncology, University of Kansas Medical Center, Kansas City, Kansas 66160, United States*

Complete contact information is available at: https://pubs.acs.org/10.1021/acs.jmedchem.0c01700

Notes

The authors declare the following competing financial interest(s): Mishra and Blagg have recently started Grannus Therapeutics in an effort to move this research towards clinical evaluation.
The authors have recently started Grannus Therapeutics to develop a similar scaffold.

■ ACKNOWLEDGMENTS

This work was supported by grants from The National Institutes of Health to CA213566 (B.S.J.B.), and the National Institutes of Health Graduate Training Grant T32GM075762 (C.N.K.). Support for the NMR instrumentation was provided by NIH Shared Instrumentation Grants (S10OD016360, S10RR024664) and NSF Major Research Instrumentation Grant (0320648).

■ ABBREVIATIONS

hERG, human ether-a-go-go-related gene; ATP, adenosine triphosphate; PDB, Protein Databank; CDK4, cyclin-dependent kinase 4; CDK6, cyclin-dependent kinase 6; cIAP1, cellular inhibitor of apoptosis protein-1; CXCR4, C-X-C motif chemokine receptor 4; Akt-1, AKT serine/threonine kinase 1; Raf-1, Raf-1 proto-oncogene; Hsf-1, heat shock transcription factor 1; Hsp70, heat shock protein 70; SNAr, nucleophilic aromatic substitution.

■ REFERENCES

(1) Sreedhar, A. S.; Kalmár, É.; Csermely, P.; Shen, Y.-F. Hsp90 isoforms: functions, expression and clinical importance. *FEBS Lett.* **2004**, *562*, 11−15.
(2) Chen, B.; Piel, W. H.; Gui, L.; Bruford, E.; Monteiro, A. The HSP90 family of genes in the human genome: insights into their divergence and evolution. *Genomics* **2005**, *86*, 627−637.
(3) Garg, G.; Khandelwal, A.; Blagg, B. S. J. Anticancer inhibitors of Hsp90 function: beyond the usual suspects. *Adv. Cancer. Res.* **2016**, *129*, 51−88.
(4) Whitesell, L.; Lindquist, S. L. HSP90 and the chaperoning of cancer. *Nat. Rev. Cancer* **2005**, *5*, 761−772.
(5) Elif Karagöz, G.; Rüdiger, S. G. D. Hsp90 interaction with clients. *Trends Biochem. Sci.* **2015**, *40*, 117−125.
(6) Röhl, A.; Rohrberg, J.; Buchner, J. The chaperone Hsp90: changing partners for demanding clients. *Trends Biochem. Sci.* **2013**, *38*, 253−262.
(7) Zuehlke, A.; Johnson, J. L. Hsp90 and co-chaperones twist the functions of diverse client proteins. *Biopolymers* **2010**, *93*, 211−217.
(8) Vaughan, C. K.; Neckers, L.; Piper, P. W. Understanding of the Hsp90 molecular chaperone reaches new heights. *Nat. Struct. Mol. Biol.* **2010**, *17*, 1400−1404.
(9) Chiosis, G.; Dickey, C. A.; Johnson, J. L. A global view of Hsp90 functions. *Nat. Struct. Mol. Biol.* **2013**, *20*, 1−4.
(10) Miyata, Y.; Nakamoto, H.; Neckers, L. The therapeutic target Hsp90 and cancer hallmarks. *Curr. Pharm. Des.* **2013**, *19*, 347−365.
(11) Trepel, J.; Mollapour, M.; Giaccone, G.; Neckers, L. Targeting the dynamic HSP90 complex in cancer. *Nat. Rev. Cancer* **2010**, *10*, 537−549.
(12) Neckers, L.; Trepel, J. B. Stressing the development of small molecules targeting HSP90. *Clin. Cancer. Res.* **2014**, *20*, 275−277.
(13) Travers, J.; Sharp, S.; Workman, P. HSP90 inhibition: two-pronged exploitation of cancer dependencies. *Drug Discovery Today* **2012**, *17*, 242−252.
(14) Bhat, R.; Tummalapalli, S. R.; Rotella, D. P. Progress in the discovery and development of heat shock protein 90 (hsp90) inhibitors. *J. Med. Chem.* **2014**, *57*, 8718−8728.
(15) Barrott, J. J.; Haystead, T. A. J. Hsp90, an unlikely ally in the war on cancer. *FEBS J.* **2013**, *280*, 1381−1396.
(16) Jhaveri, K.; Taldone, T.; Modi, S.; Chiosis, G. Advances in the clinical development of heat shock protein 90 (Hsp90) inhibitors in cancers. *Biochim. Biophys. Acta* **2012**, *1823*, 742−755.
(17) Khandelwal, A.; Crowley, V. M.; Blagg, B. S. J. Natural product inspired N-terminal Hsp90 inhibitors: from bench to bedside? *Med. Res. Rev.* **2016**, *36*, 92−118.
(18) Neckers, L.; Workman, P. Hsp90 molecular chaperone inhibitors: are we there yet? *Clin. Cancer Res.* **2012**, *18*, 64−76.
(19) Garcia-Carbonero, R.; Carnero, A.; Paz-Ares, L. Inhibition of Hsp90 molecular chaperones: moving into the clinic. *Lancet Oncol.* **2013**, *14*, e358−e369.
(20) Biamonte, M. A.; Van de Water, R.; Arndt, J. W.; Scannevin, R. H.; Perret, D.; Lee, W. C. Heat shock protein 90: inhibitors in clinical trials. *J. Med. Chem.* **2010**, *53*, 3−17.
(21) Hong, D. S.; Banerji, U.; Tavana, B.; George, G. C.; Aaron, J.; Kurzrock, R. Targeting the molecular chaperone heat shock protein 90 (HSP90): lessons learned and future directions. *Cancer Treat. Rev.* **2013**, *39*, 375−387.
(22) Powers, M. V.; Workman, P. Inhibitors of the heat shock response: biology and pharmacology. *FEBS Lett.* **2007**, *581*, 3758−3769.
(23) (a) Peterson, L. B.; Eskew, J. D.; Vielhauer, G. A.; Blagg, B. S. J. The hERG channel is dependent upon the Hsp90α isoform for maturation and trafficking. *Mol. Pharmaceutics* **2012**, *9*, 1841−1846. (b) Wu, Y.; Zheng, X.; Ding, Y.; Zhou, M.; Wei, Z.; Liu, T.; Liao, K. The molecular chaperone Hsp90a; deficiency causes retinal degeneration by disrupting Golgi organization and vesicle transportation in photoreceptors. *J. Mol. Cell Biol.* **2020**, *12*, 216−229.
(24) Bagatell, R.; Paine-Murrieta, G. D.; Taylor, C. W.; Pulcini, E. J.; Akinaga, S.; Benjamin, I. J.; Whitesell, L. Induction of a heat shock factor 1-dependent stress response alters the cytotoxic activity of hsp90-binding agents. *Clin. Cancer. Res.* **2000**, *6*, 3312−3318.
(25) Jolly, C.; Morimoto, R. I. Role of the heat shock response and molecular chaperones in oncogenesis and cell death. *J. Natl. Cancer Inst.* **2000**, *92*, 1564−1572.
(26) Butler, L. M.; Ferraldeschi, R.; Armstrong, H. K.; Centenera, M. M.; Workman, P. Maximizing the therapeutic potential of HSP90 inhibitors. *Mol. Cancer Res.* **2015**, *13*, 1445−1451.
(27) Panaretou, B.; Prodromou, C.; Roe, S. M.; O'Brien, R.; Ladbury, J. E.; Piper, P. W.; Pearl, L. H. ATP binding and hydrolysis are essential to the function of the Hsp90 molecular chaperone in vivo. *EMBO J.* **1998**, *17*, 4829−4836.
(28) Prince, T. L.; Kijima, T.; Tatokoro, M.; Lee, S.; Tsutsumi, S.; Yim, K.; Rivas, C.; Alarcon, S.; Schwartz, H.; Khamit-Kush, K.; Scroggins, B. T.; Beebe, K.; Trepel, J. B.; Neckers, L. Client proteins and small molecule inhibitors display distinct binding preferences for constitutive and stress-induced HSP90 isoforms and their conformationally restricted mutants. *PLoS One* **2015**, *10*, e0141786−e0141786.
(29) Zubrienė, A.; Gutkowska, M.; Matulienė, J.; Chaleckis, R.; Michailovienė, V.; Voroncova, A.; Venclovas, Č.; Zylicz, A.; Zylicz, M.; Matulis, D. Thermodynamics of radicicol binding to human Hsp90 alpha and beta isoforms. *Biophys. Chem.* **2010**, *152*, 153−163.
(30) Gewirth, D. T. Paralog specific Hsp90 inhibitors - a brief history and a bright future. *Curr. Top. Med. Chem.* **2016**, *16*, 2779−2791.

(31) Lee, C.; Park, H. K.; Jeong, H.; Lim, J.; Lee, A. J.; Cheon, K. Y.; Kim, C. S.; Thomas, A. P.; Bae, B.; Kim, N. D.; Kim, S. H.; Suh, P. G.; Ryu, J. H.; Kang, B. H. Development of a mitochondria-targeted Hsp90 inhibitor based on the crystal structures of human TRAP1. *J. Am. Chem. Soc.* **2015**, *137*, 4358−4367.
(32) Patel, P. D.; Yan, P.; Seidler, P. M.; Patel, H. J.; Sun, W.; Yang, C.; Que, N. S.; Taldone, T.; Finotti, P.; Stephani, R. A.; Gewirth, D. T.; Chiosis, G. Paralog-selective Hsp90 inhibitors define tumor-specific regulation of HER2. *Nat. Chem. Biol.* **2013**, *9*, 677−684.
(33) (a) Duerfeldt, A. S.; Peterson, L. B.; Maynard, J. C.; Ng, C. L.; Eletto, D.; Ostrovsky, O.; Shinogle, H. E.; Moore, D. S.; Argon, Y.; Nicchitta, C. V.; Blagg, B. S. J. Development of a Grp94 inhibitor. *J. Am. Chem. Soc.* **2012**, *134*, 9796−9804. (b) Crowley, V. M.; Khandelwal, A.; Mishra, S.; Stothert, A. R.; Huard, D. J. E.; Zhao, J.; Muth, A.; Duerfeldt, A. S.; Kizziah, J. L.; Lieberman, R. L.; Dickey, C. A.; Blagg, B. S. J. Development of glucose regulated protein 94-selective inhibitors based on the BnIm and Radamide scaffold. *J. Med. Chem.* **2016**, *59*, 3471−3488.
(34) Mishra, S. J.; Ghosh, S.; Stothert, A. R.; Dickey, C. A.; Blagg, B. S. J. Transformation of the non-selective aminocyclohexanol-based Hsp90 inhibitor into a Grp94-seletive scaffold. *ACS Chem. Biol.* **2016**, *12*, 244−253.
(35) Khandelwal, A.; Kent, C. N.; Balch, M.; Peng, S.; Mishra, S. J.; Deng, J.; Day, V. W.; Liu, W.; Subramanian, C.; Cohen, M.; Holzbeierlein, J. M.; Matts, R.; Blagg, B. S. J. Structure-guided design of an Hsp90β N-terminal isoform-selective inhibitor. *Nat. Commun.* **2018**, *9*, 425.
(36) Ernst, J. T.; Liu, M.; Zuccola, H.; Neubert, T.; Beaumont, K.; Turnbull, A.; Kallel, A.; Vought, B.; Stamos, D. Correlation between chemotype-dependent binding conformations of HSP90α/β and isoform selectivity-Implications for the structure-based design of HSP90α/β selective inhibitors for treating neurodegenerative diseases. *Bioorg. Med. Chem. Lett.* **2014**, *24*, 204−208.
(37) Kim, J.; Felts, S.; Llauger, L.; He, H.; Huezo, H.; Rosen, N.; Chiosis, G. Development of a fluorescence polarization assay for the molecular chaperone Hsp90. *J. Biomol. Screen.* **2004**, *9*, 375−381.
(38) Ernst, J. T.; Neubert, T.; Liu, M.; Sperry, S.; Zuccola, H.; Turnbull, A.; Fleck, B.; Kargo, W.; Woody, L.; Chiang, P.; Tran, D.; Chen, W.; Snyder, P.; Alcacio, T.; Nezami, A.; Reynolds, J.; Alvi, K.; Goulet, L.; Stamos, D. Identification of novel HSP90α/β isoform selective inhibitors using structure-based drug design. demonstration of potential utility in treating CNS disorders such as Huntington's disease. *J. Med. Chem.* **2014**, 3382−3400.
(39) Slamon, D. J.; Clark, G. M.; Wong, S. G.; Levin, W. J.; Ullrich, A.; McGuire, W. L. Human breast cancer: correlation of relapse and survival with amplification of the HER-2/neu oncogene. *Science* **1987**, *235*, 177−182.
(40) Stern, D. F.; Heffernan, P. A.; Weinberg, R. A. p185, a product of the neu proto-oncogene, is a receptorlike protein associated with tyrosine kinase activity. *Mol. Cell. Biol.* **1986**, *6*, 1729−1740.
(41) Moasser, M. M. The oncogene HER2; Its signaling and transforming functions and its role in human cancer pathogenesis. *Oncogene* **2007**, *26*, 6469−6487.

https://dx.doi.org/10.1021/acs.jmedchem.0c01700
J. Med. Chem. 2021, 64, 1545−1557